Membraneless Water Purification via Diffusiophoresis

By

Shicheng Lyu

A Thesis

Submitted to the Faculty

Of the

WORCESTER POLYTECHNIC INSTITUTE
In partial fulfillment of the requirements for the

Degree of Master of Science

In

Chemical Engineering

April 18, 2019A

APPROVED:

_____

Assistant Professor Andrew R. Teixeira, Thesis Advisor

_____

Assistant Professor Elizabeth J. Stewart, Thesis Advisor

_____

Professor Anthony G. Dixon, Thesis Committee Member

_____

Professor Harold W. Walker, Thesis Committee Member

Abstract

Clean water is hard to obtain in certain areas, such as remote locations and during emergency response. Our study developed a membraneless water purification system using diffusiophoresis and tested the influence of various factors (gas pressure, liquid flow rate, etc.) on the turbidity of filtered water. The main component in the separation system is a tube-in-tube-in-tube separator. The inner tube and the middle tube are made of a semipermeable material (Teflon AF-2400), which allows gas (CO_2) to permeate through it, but retains liquid (water). In this strategy, the CO_2 permeates through the inner tube (the end is sealed) then dissolves into the dirty water/particle suspension passing through the middle tube. It then diffuses radially to the outer tube, where a vacuum collects the CO_2, forming a concentration gradient of ions through the water, which induces the migration of charged particles to concentrate at the inner wall of the middle tube. The vacuum phase in the outer tube can increase the concentration gradient of ions in the water and recycle the CO_2. Finally, purified water can be collected from the center of the middle tube by a needle in the effluent. The purification system is able to take initial turbid water (243 NTU) to below the WHO drinking water standard (<5 NTU). Compared with standard water filtration methods, our system only needs electricity to operate and does not require filter regeneration or replacement.

Acknowledgements

I would like to take this opportunity to express a deep thanks to Prof. Teixeira, Prof Stewart, Prof. Paulsen, Tom Partington, Cameron Armstrong and Mainstream Engineering Corporation. I could not finish my project without your guidance, supports and resources. Special thanks to my labmates both in Teixeira Lab and Timko Lab for their patient help. I feel fortunate to be part of the department, who brought me a lot of happy moments, and Great thanks for the support and encouragement from my family and friends in the last two years.

Thanks again to everyone.

Table of Contents

List of Figures.

List of Tables.

1.0 Introduction.

1.1 Motivation for Distributed, Clean Water

Freshwater is one of the most important resources for all societal activities and ecology. Whether it is industrial development and human health, food and energy production, all industries need water to operate. With the population growth, climate change and water pollution, water shortage is critical in some regions of the world. Even in certain areas, water acted as the catalyst to accelerate the region conflict[1].

The earth has a huge amount of water. However, most water is in the ocean, 97% of water is saline water, and cannot be easily used. Of the remaining amount, 2.5% is freshwater. But large portion (67%) is held up as ice and snow in the mountainous area, the Arctic, and the Antarctic. The remaining freshwater is groundwater and surface water in the form of lakes, rivers, and reservoirs. This water can be used as a potable source of industrial and agricultural purposes, but often needs treatment first.

Expected changes to the global climate coupled with water pollution, and slow replenishment due to high demands, all lead to water scarcity. Oceanic water needs 2,500 years to replenish; permafrost and polar ice need 10,000 years and 1,500 years for mountain glaciers and deep ground water. Water in the lakes need 17 years to be fully replenished[2].

In certain regions of the world, some countries are facing critical water shortages and pollution. Pakistan is one of them. The main reasons for water shortage in Pakistan are climate conditions, water pollution, poor water treatment system, and endless war. The climate condition and water pollution prevent Pakistan from getting plenty of water. The poor water treatment systems means their government does not have the ability to provide clean water to every citizen[3]. Pakistan is not the only one country that has been in this

critical situation. Sub-Saharan Africa faces demands that are compounded by extreme weather-related shortages and lack of infrastructure.

All of these challenges for achieving clean drinking water necessitate and motivate the need for small, easy-to-install devices that are better suited for these places; these kinds of devices are also suitable for those families who cannot rely on clean water from public water systems.

1.2 Traditional Methods of Water Treatment.

Traditional methods for water treatment rely on physical, chemical, and biological methods. Physical methods include filtration, sedimentation, and distillation. Chemical processes include flocculation and chlorination, for example. Biological processes such as anaerobic digestion or biologically active carbon filtration can also be used to purify water. These water treatment processes are often accompanied by high costs, chemical infrastructure (i.e., reagent supply, filters, etc.) large footprints, and regular maintenance.
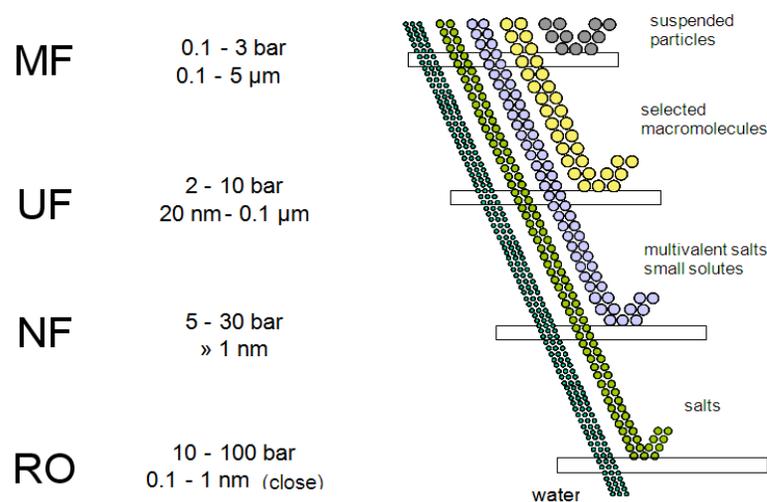
Figure 1. Common filtration methods utilize increasingly smaller pore size filters to reject particle fractions, leading to a clean permeate. Smaller pore sizes result in membrane fouling and extreme pressure drops. Adapted from VITO-SCT et al. [4].

Small-scale water treatment systems typically rely on membranes and filters to remove suspended contaminants from dirty water. Like the filtration methods in the figure 1, large holes have less pressure drop but can only block big particles, while small holes can block small particles but have high-pressure drop and can be easily clogged. The filters and membranes of these kinds of technologies will be fouled and replaced regularly, and the cost of membrane replacement is the key cost factor for the water treatment plant. It will take 10 to 30 percent of the total cost, which includes the cost of annualized capital, feed power, labor, etc[5]. In contrast, our system uses a membaneless approach for performing the same physical separation; if working properly, the device has no consumable parts and recycles CO_2, so it only needs electricity to operate.

2.0 Background

2.1 Diffusiophoresis.

Diffusiophoresis is a transport phenomenon process that results in the spontaneous motion of charged suspended particles induced by the concentration gradient of a second oppositely charged species. It can be used to separate particles with very low energy consumption.

The first step in the process is to generate the charge gradient with our second species, carbon dioxide (CO_2). The gas first undergoes dissolution and dissociation upon contact with the water, as described by:

Table1. Equilibrium equation and constant of CO_2-Water. Adapted from Greenwood et al[6].

Equilibrium Equation	Equilibrium Constant
$CO_2(g) + H_2O(l) \rightleftharpoons H_2CO_3(aq)$	$K_h = \dfrac{[H_2CO_3]}{[CO_2]} \approx 1.7 \times 10^{-3}(25°C)$
$H_2CO_3(aq) \rightleftharpoons HCO_3^-(aq) + H^+(aq)$	$Ka_1 = \dfrac{[H^+][HCO_3^-]}{[H_2CO_3]} \approx 2.5 \times 10^{-4}(25°C)$
$HCO_3^-(aq) \rightleftharpoons CO_3^{2-}(aq) + H^+(aq)$	$Ka_2 = \dfrac{[CO_3^{2-}][H^+]}{[HCO_3^-]} \approx 4.69 \times 10^{-11}(25°C)$

After CO_2 dissociates into carbonic acid (hydronium, bicarbonate and carbonate), The concentration of CO_2 in the water at the interface is constant and determined by the gas pressure of CO_2. From here, we can determine the concentration of hydronium, bicarbonate and carbonate by the equilibrium constant of each reaction. Because the Ka_2 is $4.69 * 10^{-11}$, the amount of carbonate is very small compared with the amount of bicarbonate, and the concentration of H^+ is much higher than carbonate and bicarbonate. These three ions then travel down gradient by Fickian diffusion[7] (Figure 2). The flux of the small hydronium is substantially faster than the carbonates, as the diffusivity of the

molecules through water scales with their size, as approximated by a small sphere moving described by Stokes' law[8].

$$D_i = \frac{k_b T}{6\pi\eta R_i}$$

Because

$$R_{H^+}(0.6\text{Å}) \ll R_{HCO_3^-}(1.56\text{Å}) < R_{CO_3^{-2}}(1.78\text{Å})$$

Therefore

$$D_{H^+} \gg D_{HCO_3^-} > D_{CO_3^{-2}}$$

In the equation of Stokes' law, D_i is the diffusivity, R_i is the radius of spherical particles, k_b is Boltzmann's constant, T is the absolute temperature, and η is the dynamic viscosity.

This causes a corresponding charge gradient felt by negatively charged particles (contaminants), that then moves by diffusiophoresis from the negatively charged zone (CO_2/water interface) to the positively charged zone where the hydronium have accumulated (outer air/water interface). The net effect is a motion of the particles with the ion gradient, referred to as diffusiophoresis.

Figure 3 shows the motion of positive/negative charged particles. If we expose the water with particles to CO_2, it will generate sufficient concentration gradients of ion in the water to drive particles move away or forward (depend on their surface charge) the interface of water and CO_2. The particles with positive charge will move toward the interface of gas and water, and the particles with negative surface charge will move away from the interface[9]. Diffusiophoresis has been studied since 1947, but only recent years

has it taken off for water treatment with major advancements by Stone and coworkers who

published "Membraneless water filtration using CO_2".
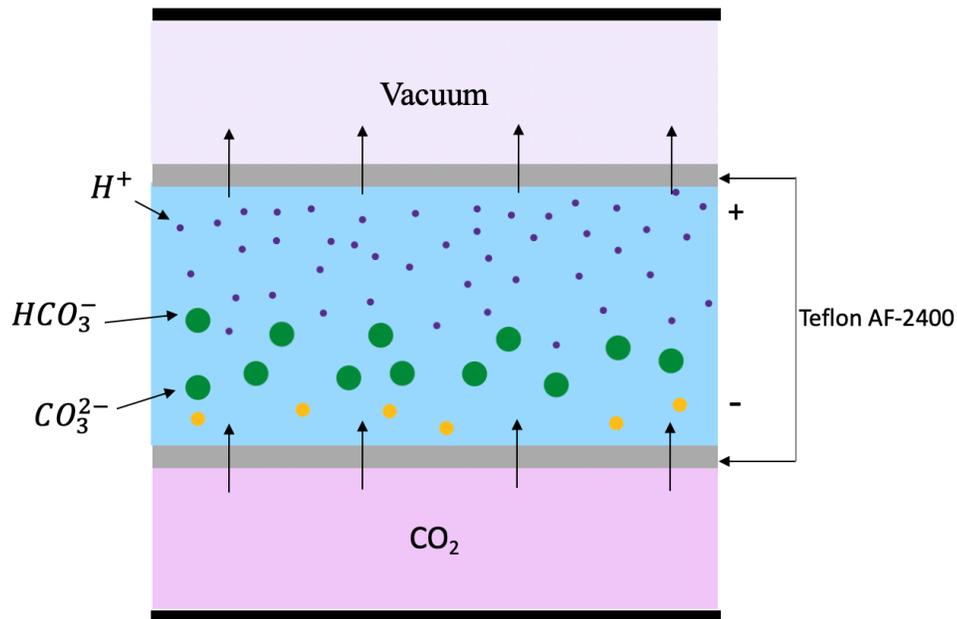
Figure 2. Motion of ions when CO_2 dissociates into water. The radius of H⁺ is much smaller than CO_3^- and HCO_3^- that causes the migration rate of H⁺ is faster than others. The field of water near the vacuum phase shows positive charge because the concentration of H⁺ is higher than others. The field of water near the CO_2 shows positive charge since the concentration of cations is higher.
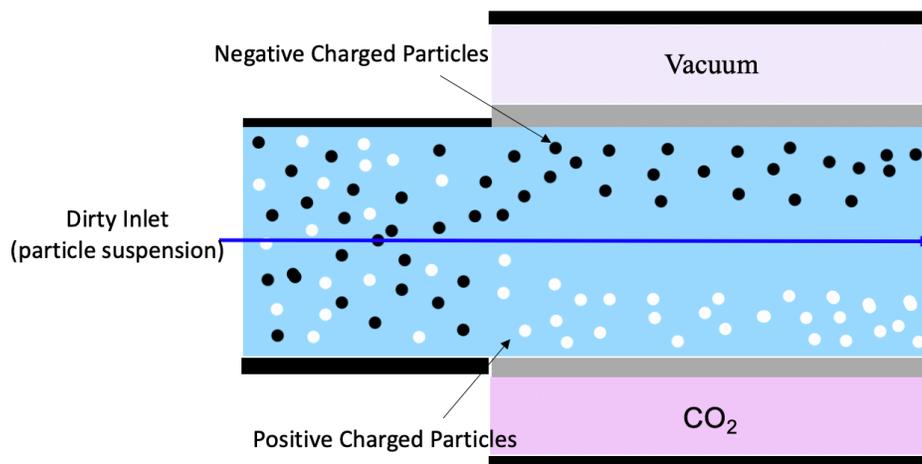
Figure 3. The motion of positive/negative charged particles in the concentration gradient of ions.

2.2 Tube-in-Tube Reactor.

Tube-in-tube (or tube-in-shell) reactors have been widely discussed for applications in flow chemistry. In this configuration, a concentric tube-in-tube geometry is constructed where the inner tube is gas-permeable, allowing for radial gas introduction through the tube wall without ever directly contacting the two phases. This has proven useful for situations where the interface needs to be well-described[10] or when safety concerns arise from the use of hazardous gases where pressurized reactor headspace cannot be used (e.g. hydrogenation, ozone oxidations, etc). To the best of our knowledge, no known applications exist for a tube-in-tube-in-tube geometry, as proposed in this thesis.

The tube-in-tube reactor is typically constructed by concentrically assembling semipermeable tube, such as PDMS and Teflon AF-2400, with an impermeable outer tube. The inner tube allows gas through it but isolates liquid. The tube-in-tube reactor is designed by this property, such as figure 4. All CO_2 permeates through the inner tube into the liquid because the end of gas supply tube is sealed downstream.
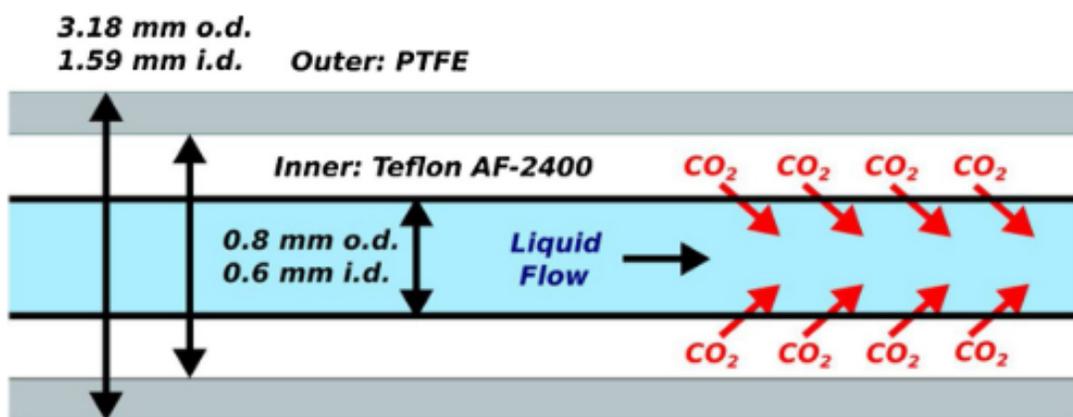
Figure 4. Basic schematic of tube-in-tube reactor. Figure adapted from L.Yang et al[11]. The CO_2 flows through the outer tube, and the liquid flows through the inner tube ,which is made of Teflon AF-2400. The CO2 flows through the inner tube then dissolves into water
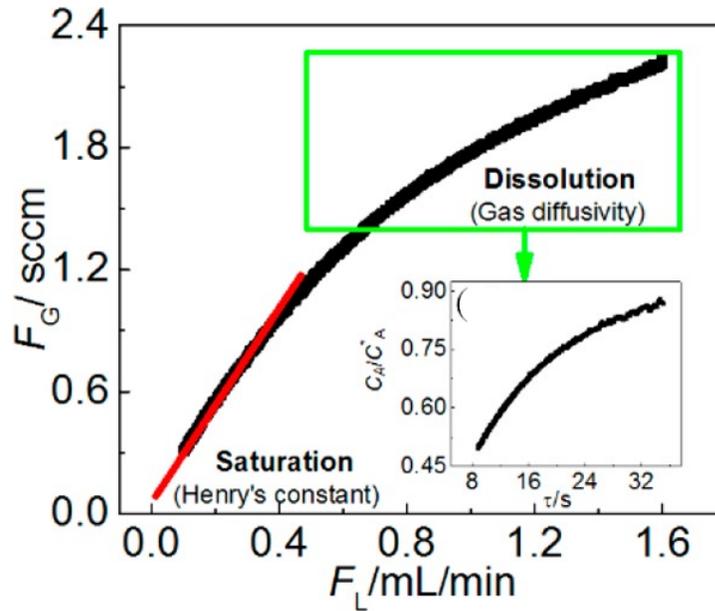
Figure 5. Measured gas flow rate of CO_2 versus liquid flow rate during the ramping process. Gas pressure: 4.1 bar; temperature, 20 °C; ramping time, 80 min. Adapted from Zhang et al and reprinted here[12].

In figure 5, the slope of the curve is the solubility of the CO_2-water system in the tube-in-tube reactor. Comparing the experimental data to the literature data (red line in the plot), the solubility of gas-liquid in tube-in-tube device is nearly identical at saturation regions, and the range of liquid flow rates of our experiments are in saturation regions. Therefore, Teflon AF-2400 won't influence the dissolution of gas-water in our system. These results were reproduced in this thesis work toward validating the base case for CO2 uptake, without diffusiophoresis. It will later be shown how it can be expanded with a second semi-permeable tube.

3.0 Methodology

3.1 Tube-in-Tube-in-Tube Separator

Our tube-in-tube-in-tube Separator is described in figure 6. The inner and middle tube of the separator are Teflon AF-2400 tubes (Biogeneral), and the outer tube is PFA (1/16" ID, 1/8" OD, 0.8m long). The CO_2 from the gas tank is fed into the inner tube, and the end of the inner tube is sealed by epoxy glue. Therefore, CO_2 in the inner tube can only pass through the Teflon-AF tube and dissolve into dirty water in the second tube. IDEX PTFE fittings were used to connect all tubing, with reducing sleeves used to seal around the innermost tube. The CO_2 in the water will form a concentration gradient of ions, which will move positive and negative particles in a certain direction based on their charge. Since particles in water tend to have a negative surface charge, particles will concentrate at the wall of the second tube, and then we can use a needle to collect clean water from the center of the second tube.

For particles in natural water systems, all particles have negative surface charge, no matter in the fresh water environment[13], or in the saltwater condition, like ocean and estuaries [14][15]. Therefore, we only need to consider how to separate negative particles from dirty water.
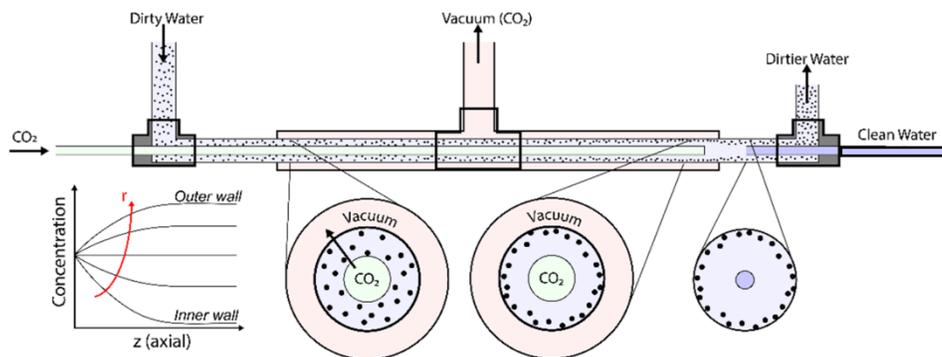
Figure 6: The schematic of the Tube-in-Tube-in-Tube separator. The inner tube and the middle tube are made of Teflon AF-2400, the outer tube is PFA tube. CO_2 from inner tube dissolve into the dirty water in the middle tube, then form concentration gradient of ion which induces the motion of particles. Then part of CO_2 will flow through the middle tube then into the outer tube and leave the separator by the vacuum. At the end of the separator, using a needle to get the clean water from the middle of the second tube.

3.2 System Design
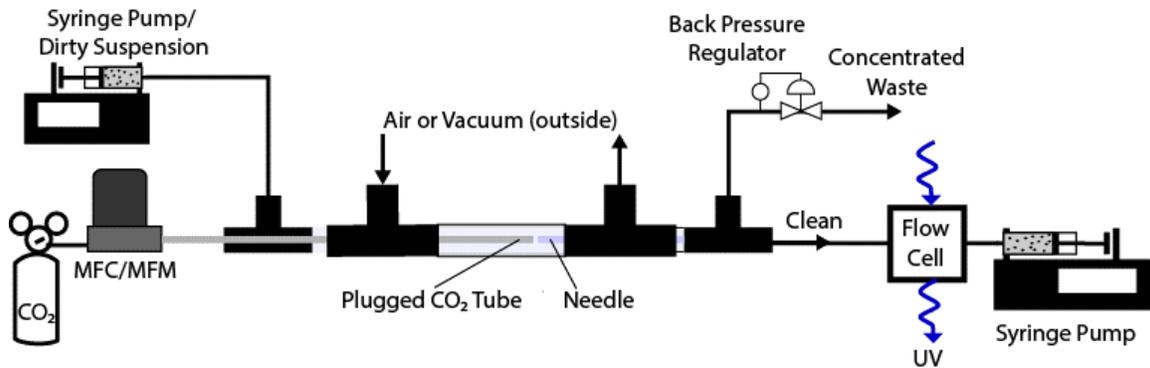
Figure 7: Schematic of the water treatment system.

Our system uses a tube-in-tube-in-tube separator to separate the particles from dirty water. In addition to the separator, the system has a syringe pump (Harvard Aparatus PHD Ultra with 60 mL plastic syringes) at the inlet of the system to pump the dirty water into the separator. For the CO_2, we used compressed gas tank and gas pressure regulator to supply and control the gas pressure of CO_2 between 150-250 kPa. The gas flow is monitored with a thermal mass flow controller (Brooks 5850, up to 30 slpm). At the end of the separator, the clean water passes through a flow cell into a syringe pump (Harvard Aparatus PHD Ultra, withdraw mode), which is used to control the flow rate of clean water. No cavitation was observed in the syringe at the low flowrates used here. A UV/Vis spectrometer (OceanOptics FLAME-S-UV-VIS-ES) is used with a high-intensity halogen/dual deuterium lamp (DH-2000-BAL) and a custom-designed flow cell to measure the turbidity of the clean water through the tube wall. The concentrated wastewater passes through a backpressure regulator (Zaiput BPR-10) into a collection beaker; the backpressure regulator is used to set the liquid pressure (160 kPa) of the separator necessary to keep CO2 dissolved in the water. A LabVIEW automation program is used to monitor and log UV intensity and gas flow rate, and control all equipment of the system.

3.3 Equipment

3.3.1 Tubing Configurations

The Teflon AF-2400 tubes are from the company Biogeneral. Table 2 shows the tubes which we used to build our current separator. We used this combination to construct the separator is because the diameters of this set of tubes are bigger than others. Because Teflon AF-2400 tubes are very fragile, the bigger diameter can make the first build process easier. Table 3 is the combinations of Teflon AF-2400 tubes we have, and we will use them to detect the influence of the separator size on the separation performance.

Table 2. The dimension of Teflon AF-2400 tubes.

	Outside Diameter mm (in)	Inside Diameter mm (in)
Inner Tube	0.74(0.029)	0.61(0.024)
Outer Tube	1.02(0.040)	0.81(0.032)

Table 3. The combinations of Teflon AF-2400 tubes we choose.

	Inner Tube		Second Tube		
	OD mm(in)	ID mm(in)	OD mm(in)	ID mm(in)	Thickness mm(in)
1	0.74(0.029)	0.61(0.024)	1.02(0.04)	0.82(0.032)	0.076(0.003)
2	0.30(0.012)	0.23(0.009)	0.74(0.029)	0.61(0.024)	0.30(0.012)
3	0.30(0.012)	0.23(0.009)	1.02(0.04)	0.82(0.032)	0.51(0.02)

3.3.2 Pump Selection

Figure 8. Harvard Apparatus PHD ULTRA Syringe pump.

Our system requires pumping of the liquid feed. Additionally, a second pump is used to extract the clean water. While a well-controlled split valve may be used in manufacturing applications, laboratory studies were performed with a second syringe pump to precisely control the split ratio. The feed pump is located at the beginning of the separator to pump the water with particles into the separator. The other one is at the end of the outlet tube of the clean water, and this pump is used to control the flow rate of clean water and adjust the ratio of clean water and wastewater. The syringe pumps are infuse/withdraw pumps, Harvard Apparatus PHD Ultra (70-3007).

We also considered using HPLC pump as a feeding pump, but HPLC pump can only be applied on pumping pure water, particle suspension will clog the pump. Finally, we choose a syringe pump as our feeding pump.

3.3.3 UV Light Source and UV Spectrometer

a

b

c
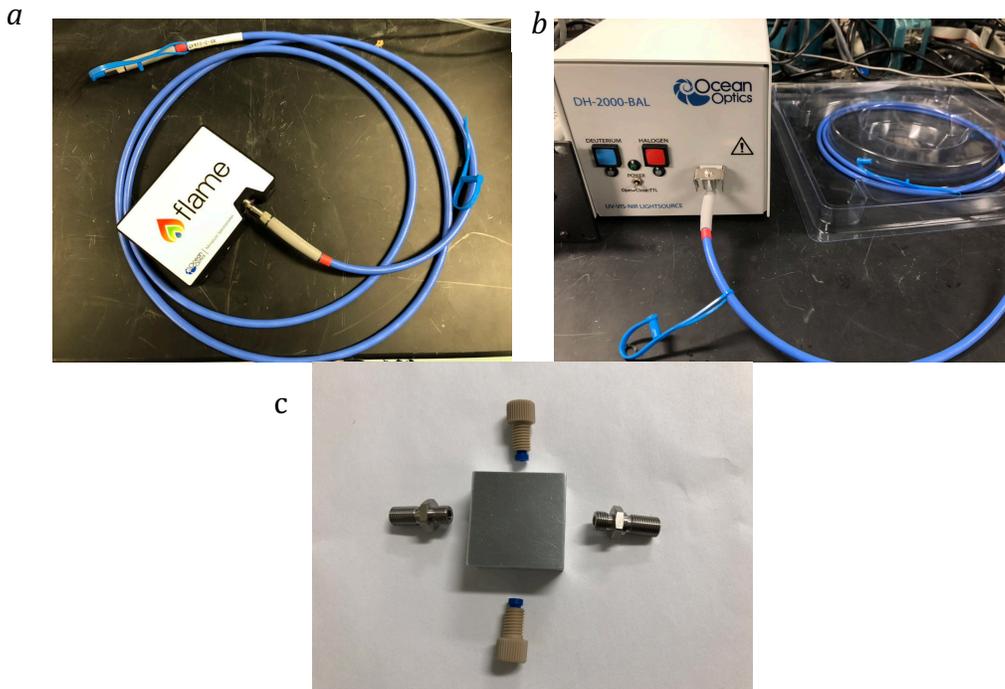
Figure 9. (a) UV light source. (b) UV spectrometer. (c) Flow cell.

After the separation process in the separator, we need to measure the turbidity of the clean water we get from the separator. Therefore, we connect the UV light source and spectrometer to a flow cell, which can let the outlet tube of the clean water through it, in this way, the turbidity of the clean water can be measured on time and continuously. The UV light source (DH-2000-BAL) and spectrometer (FLAME-S-UV-VIS-ES) are from the company Ocean Optics.

For the light source, we use dual deuterium-halogen light to provide a broad-spectrum, the high power of the light source allows transmission through the PFA tubing.

3.3.4 Mass Flow Controller
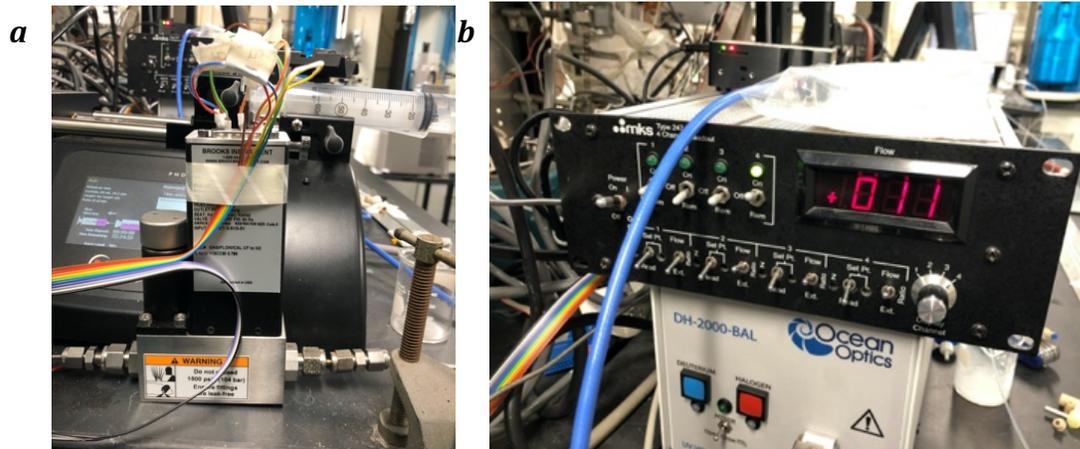
Figure 10. (a) Mass flow controller. (b) Power supply of mass flow controller.

The mass flow controller is connected with the gas tank of CO_2 to adjust the gas flow rate

of the CO_2. The main function of the power supply is to control the mass flow controller and read

the voltage signal from the mass flow controller. By using a bubble meter, we got the calibration

curve, which can convert the voltage signal to the gas flow rate. The mass flow controller is from

the company Brooks (5850). The power supply is from the company MKS (247).

For the calibration curve of gas flow rate, we connect the mass flow controller to a bubble

meter, then read and record the gas flow rate by the bubble meter under different voltage signals

of the mass flow controller. By corresponding the voltage signal and gas flow rate, we can get a

calibration curve (Figure 11).
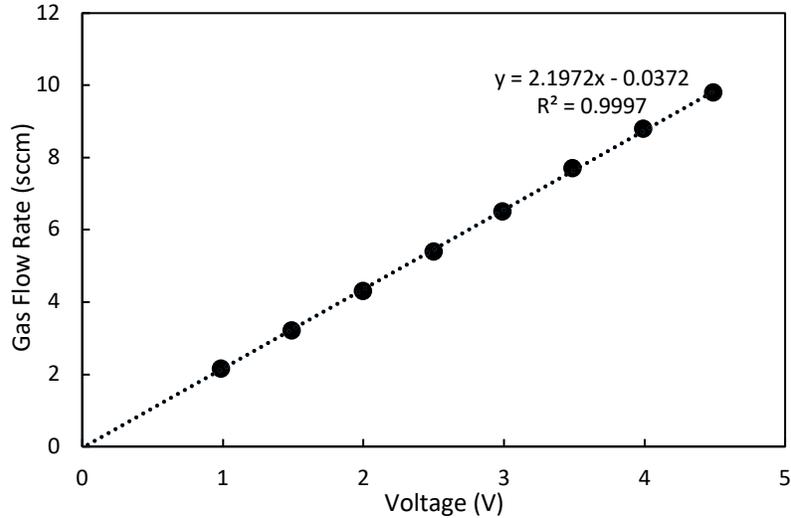
Figure 11. Calibration curve of gas flow rate. The voltage value is from the mass flow controller and recorded by computer, the gas flow rate is read by bubble meter.

3.3.5 *BackPressure Regulator*

Our system has a backpressure regulator, which is assigned at the end of the outlet tube of wastewater. This backpressure regulator is used to control the liquid pressure of the separator. Since the gas pressure of CO_2 in the inner tube is higher than the atmospheric pressure, therefore, CO_2 will appear in the form of bubbles in the water if the liquid pressure of water is not high enough. The pressure of the backpressure regulator is adjusted by the gas tank. We connect it to a gas tank of compressed air, then set the pressure on the gas tank to control the backpressure regulator. The backpressure regulator is from the company Zaiput (BPR-10).
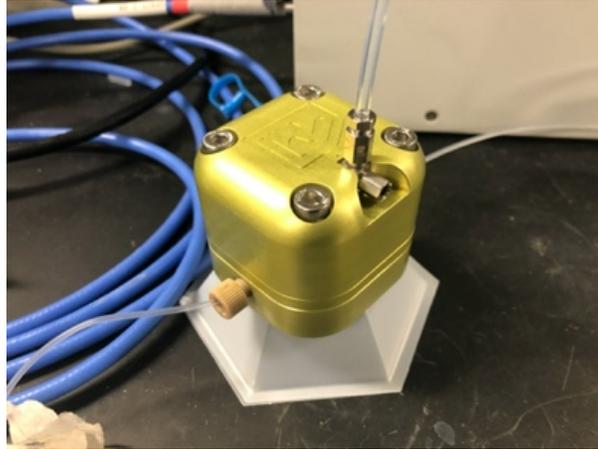
Figure 12. backpressure regulator.

3.3.6 *Tubing Fittings and Adapters*

We have some accessories to set up the system, like sleeves, tee assemblies and ferrules, etc. These accessories are from the company IDEX Health & Science.

3.4 Method of Turbidity Measurement.

In our system, we have a pair of UV light source and UV detector to measure the turbidity of the clean water. They are connected to a flow cell, when liquid flows through the flow cell, we can read the absorption value on the computer by the UV detector. By using the calibration curve, we can convert the value of absorption to turbidity.

For the calibration curve, we use a chemical method to make standard solutions. These solutions have certain turbidity. We can read the corresponding absorption value from the UV detector by injecting the standard solutions into the flow cell. Then we can get the calibration curve of absorption and turbidity (figure 13).

The standard solution is made by solution 1 (hexamethylenetetramine solution) and solution 2 (hydrazine sulfate solution). Solution 1 is made by dissolving 10.0 g hexamethylenetetramine in DI water (demineralized water) and dilute to 100 ml. Solution 2 is

prepared by dissolving 1.0 g $(NH_2)_2)\bullet H_2SO_4$ in DI water and dilute to 100 ml. Then mix 5.0 ml

solution 1 and 5.0 ml solution 2 in a 100.0 ml volumetric flask. After waiting for 24 h at room

temperature, dilute to 100.0 ml by DI water and mix well, we get 100.0 ml standard solution, which

has 40 NTU. Then we can dilute the standard solution to any turbidity we want[16].

We performed a fresh calibration curve after every time each experiment to account for

reduction in transmittance due to minor particle adhesion to the wall of the middle tube. Therefore,

making the calibration curve every time can make the data more accurate.
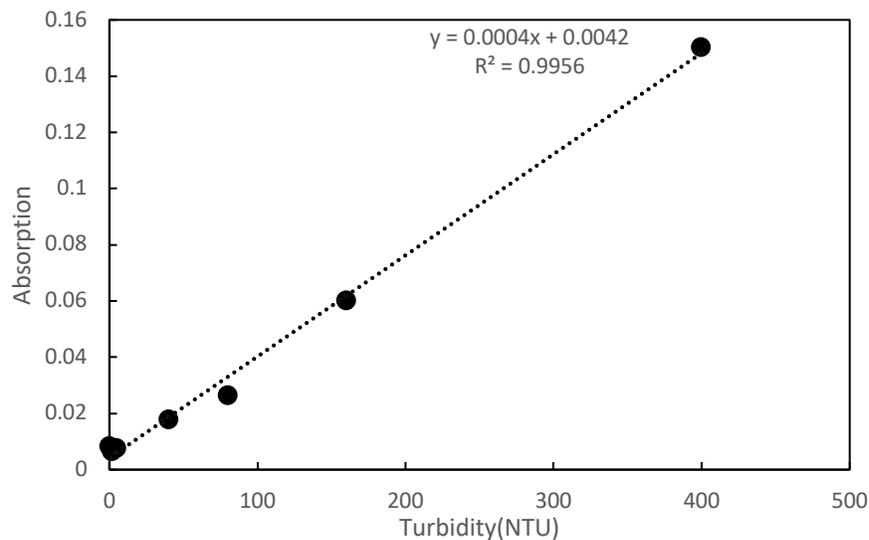
Figure 13. Calibration curve of turbidity and absorption.

3.5 Lab Grade Water

In our study, the assuming is all contaminants with positive/negative surface charges can

be removed by diffusiophoresis. Therefore, we used the particle suspension to test the system to

see if our system can work as our assumption.

The particle suspension we used in experiments is made by mixing the particle solution

and DI water. Monodisperse polystyrene particles ware obtained from Bangs

Laboratory(PS03001).

Table 4 shows the composition on ingredients of the particle solution we obtained from Bangs Laboratory.

Table 4. Composition on Ingredients.

Item#	Name	% in Product
1	Water	$\geq$ 89.41
2	Polystyrene	$\leq$ 10
3	Tween® 20	$\leq$ 0.5
4	Sodium azide	$\leq$ 0.09

.

The diameter of our particles is 0.5 μm. This number is in the middle of the diameter range of colloid particles. Particles with diameter 1 nm – 1000 nm are called colloidal particles. Colloidal particles often remain in a relatively stable suspended state in water and cannot be directly removed from the water by sedimentation[17][18]. In nature's water system, colloidal particles can act as transfer media to deliver contaminants in the water system, such as rivers, lakes, seawater, and underground water[19][20]. Different types of colloids in nature environments are divided into inorganic colloids and organic colloids. As transfer media, colloidal particles can easily absorb radionuclides and heavy metals, then transfer these contaminants in the water system[21].

In addition to the polystyrene particles, we also briefly tested bacteria in our separator with a shorter length than the current system; the bacteria was also removed by our system successfully.

3.6 COMSOL Simulation

Computational fluid mechanics simulations were performed to describe the concentration gradients within the tubes. The simulation software we used was COMSOL Multiphysics 5.5, it

can simulate the system under different physics conditions. By constructing the model of our separator, we can get the data of the diffusion and concentration distribution of CO_2.

3.6.1 Model Construction

In our system, in order to evaluate the diffusion and concentration distribution of CO_2, we need to consider two main transfer processes. The first one is the CO_2 from the inner tube through the water then into the vacuum phase in the outer tube along the radial direction, the other one is the fluid flow of water along the axial direction, as the schematic in figure 14.

Large surface area and small cross-section size enable the Teflon AF-2400 tubing to have a relatively high gas diffusion rate across the membrane. Previous studies by Jensen and coworkers[22] have rigorously demonstrated that the transport resistance of CO2 through Teflon-AF is very low compared to the diffusion through the water. For that reason, negligible transport resistance is assumed here, allowing for gas/liquid equilibrium to hold true at the interface. Therefore, we can simplify the separator to a 2-dimension model, which only has the layer of water. Using this model, we can simulate the real condition by setting the boundary condition of each side[22][23].
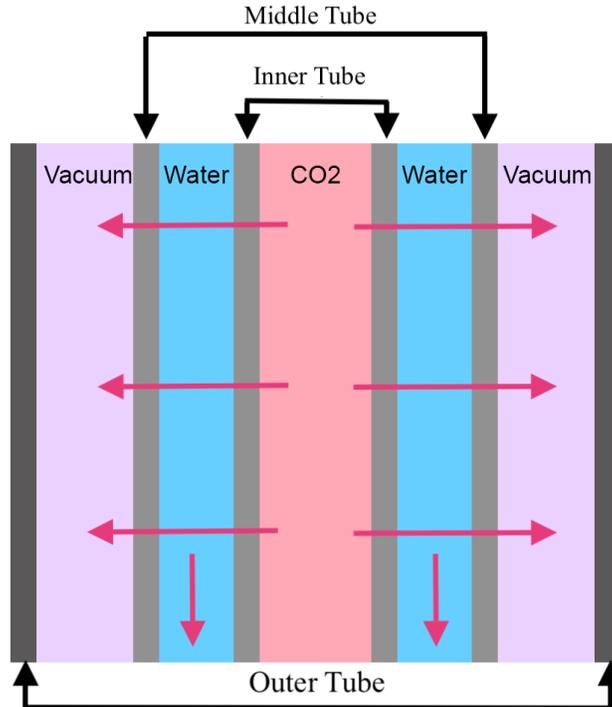
Figure 14. The vertical section of the separator. The CO_2 from the inner tube permeates through the tube wall into water, and then most CO_2 flows through the wall of the middle tube into the vacuum in the outer tube; The rest of CO_2 leaves the separator by water flow.

After simplification, the separator can be built as a rectangle and the material of it is water (figure 15). The dimension of this model is determined by the dimension of the separator in the lab. The length is 0.8m, and the width is equal to the water layer between the inner tube and the middle tube, which is 0.00074m.
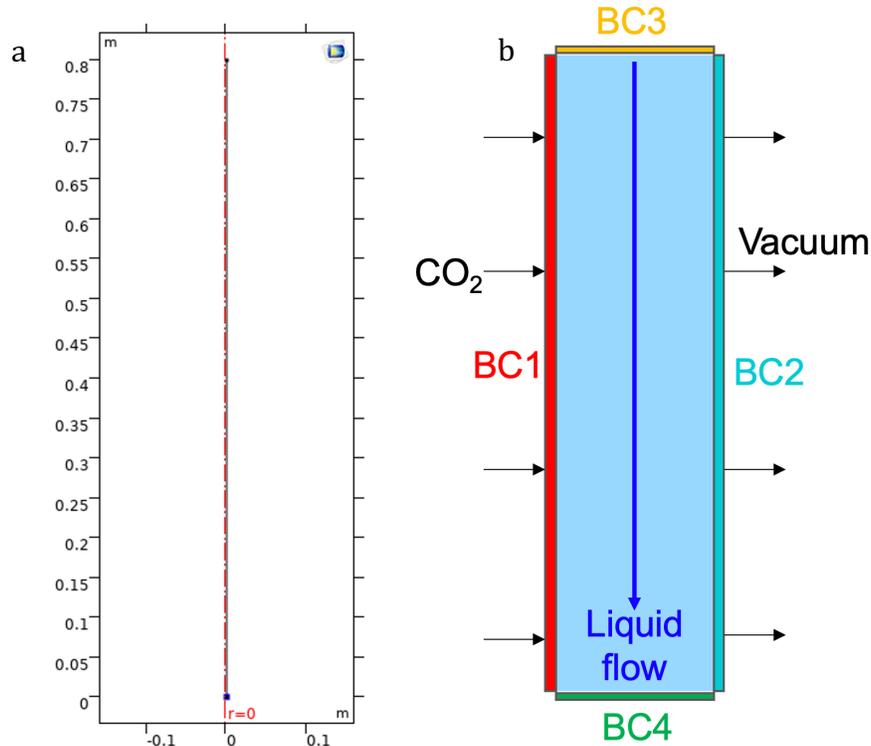
Figure 15. COMSOL Model of the system. The length is 0.8m; The width is 0.00074m (a) The schematic of the model. (b) Zoom-in image of the model. The water flows through the system from the top to the bottom. The boundary condition of the left side is determined by the gas pressure of CO_2 in the inner tube. The boundary condition of the right side is controlled by the vacuum pressure in the outer tube.

3.6.2 Boundary Condition

In order to simulate the real condition and compare the simulation result with the experimental data we got in the lab, the boundary condition of each side is the same as the experiments we did in the lab.

There are several variables, which need to be controlled, the concentration of CO_2 at the left side and the right side of the model, the liquid flow rate flow through the system, the liquid pressure of the separator.

The concentrations of CO_2 at the left side and the right side is controlled by the gas pressure of CO_2 in the inner tube and vacuum phase in the outer tube. Therefore, in the simulation, we used

Henry's law to convert the gas pressure, what we used in the experiments, to the concentration of the CO_2 in the water. The Henry's law constants are published by Sander[24].

Table 5. Henry's law constants (gases in water at 298.15k)

Gas	$K_H^{pc} = \dfrac{p}{c_{aq}}$ $\left(\dfrac{L*atm}{mol}\right)$	$H^{cp} = \dfrac{c_{aq}}{p}$ $\left(\dfrac{mol}{L*atm}\right)$	$K_H^{px} = \dfrac{p}{x}$ (atm)	$H^{cc} = \dfrac{c_{aq}}{c_{gas}}$ (dimensionless)
O_2	700	$1.3*10^{-3}$	$4.3*10^{4}$	$3.2*10^{-2}$
H_2	1300	$7.8*10^{-4}$	$7.1*10^{4}$	$1.9*10^{-2}$
CO_2	29	$3.4*10^{-2}$	$1.6*10^{3}$	$8.3*10^{-1}$
N_2	1600	$6.1*10^{-4}$	$9.1*10^{4}$	$1.5*10^{-2}$
He	2700	$3.7*10^{-4}$	$1.5*10^{5}$	$9.1*10^{-3}$
Ne	2200	$4.5*10^{-4}$	$1.2*10^{5}$	$1.1*10^{-2}$
Ar	710	$1.4*10^{-3}$	$4.0*10^{4}$	$3.4*10^{-2}$
CO	1100	$9.5*10^{-4}$	$5.8*10^{4}$	$2.3*10^{-2}$

The experiments we did in the lab at the room temperature. Therefore, we can use the equation and Henry's law constant of CO_2 from the Table 5. By inserting the partial pressure of CO_2 and Henry's law constant into an equation, the concentration of CO_2 in the water at the left side and the right side of the model can be calculated. Therefore, the boundary conditions of the left side and the right side are the concentration of CO_2 in the water.

The laminar flow was solved by defining the boundary condition of the bottom and the top of the model, because the water enters and leaves the system from the bottom to the top. The physical properties (density, viscosity) of the model were taken from water.

The edge of the top is defined by the liquid flow rate we used in the experiments, and the bottom is set by the liquid pressure, the value is constant and equal to the number of backpressure regulator.

In the COMSOL, the Multiphysics problem is solved by Transport of Diluted Species package and Laminar Flow package.

Laminar Flow Package
This package is used to simulate the laminar flow in the system. The equations are:

$$\underbrace{\rho\left(\frac{\partial u}{\partial t} + u \cdot \nabla u\right)}_{1} = \underbrace{-\nabla p}_{2} + \underbrace{\nabla \cdot \left(\mu(\nabla u + (\nabla u)^{\mathsf{T}}) - \frac{2}{3}\mu(\nabla \cdot u)I\right)}_{3} + \underbrace{F}_{4}$$

Where u is the velocity of the fluid.

P is the fluid pressure.

ρ is the density of the fluid.

μ is the viscosity of the fluid.

T is the temperature.

∇ is the divergence.

In the equation, term (1) corresponds to the inertial forces, term (2) is pressure forces, term (3) is viscous forces and (4) is the external forces.

In the domain, the left (BC 1) and the right (BC 2) sides are the inner tube, and the outer tube where liquid cannot flow through. The only flow direction of liquid is from the top (BC 3) to the bottom (BC 4). Therefore, the liquid flow rate of boundary conditions 1 and 2 are 0 ml/min. The boundary condition 3 is defined by the liquid flow rate we used in the experiments divided by the cross-sectional area of the inlet. The BC 4 is set as the liquid pressure in the experiments,

maintained by the backpressure regulator (160kPa). The system is in hydrodynamic steady state ,

so no transients to the velocity profile are considered.

Transport of Diluted Species Package

This package is used to simulate the diffusion of CO_2 based on the equations:

$$\nabla \cdot J_i + u \cdot \nabla c_i = R_i$$

$$J_i = -D_i \nabla c_i$$

J is the diffusion flux, and the dimension is the amount of substance per unit area per unit

time

∇ is the del or gradient operator, which is used to generalize the first derivative in two or

more dimensions.

D is the diffusion coefficient of CO_2 dissolve into water.

c is the concentration of CO_2.

R is a net volumetric source, which is a mass balance on the CO_2 within the control volume.

u is the velocity field, which is defined by the Laminar Flow package.

The first equation is a continuity equation, saying all the mass coming into the system must

also exit within any control volume. The second one is Fick's law, which describes the diffusion

flux in the domain. Gradients are allowed in both radial and axial directions, though later it is

observed that the radial flux dominates for the bulk of the separator.

Our domain has four boundary conditions, two of them on the radial direction and two of

them on the axial (from the top to the bottom) direction. In the radial direction, the CO_2 from the

inner tube dissociates into the water and then leaves the water into the vacuum. Therefore, the

concentration of CO_2 goes down along the r-direction. In the z-direction, the pure water enters the system from the top (z = 0) and leave the system from the bottom (z = L); the CO_2 dissociates into water during the process. Therefore, the concentration of CO_2 is zero at the top then goes up and reaches a steady-state after a short length.

For the boundary condition 1 (BC 1) and boundary condition 2 (BC 2) in the r-direction, they are determined by the concentration of CO_2 in the water in equilibrium with the gas pressure of CO_2 in the inner tube and outer gas tubes, respectively.

The boundary 3 is an inlet boundary of CO_2, but the concentration is zero because only pure water enters the separator from here. This is assumed to be void of CO_2 due to degassing prior to experiments, though real groundwater may be dilute in CO2 (equilibrium with air), or high concentration (equilibrium with carbonate minerals in the ground). The boundary 4 is an outlet boundary of CO_2, the concentration depends on how much CO_2 leaves the system with the liquid flow.

3.6.3 Mesh Refinement

COMSOL is based on the finite element method (FEM), which is widely applied to address engineering problems and mathematical problems. The FEM separates the whole system into small and simple parts that are named finite elements. This is achieved by the construction of the mesh of the object based on particular space discretization in the space dimensions. The establishment of the finite element method for boundary value problems results in an algebraic system of equations. The method approximates the unknown function in the domain. By assembling the simple equations, which are used to simulate the finite elements, into a large system of equation to simulate the whole system. In order to minimize the error, the FEM uses variational methods to estimate the result[25].

Therefore, after defining the boundary conditions of the model, we need to select a suitable element size of the mesh to do the simulation. In the COMSOL, element size has eight levels from extremely coarse to extremely fine that are showed in figure 16. Obviously, finer mesh will bring us a more accurate result of simulation, but it will increase amount of calculation on the computer and take more time to finish the simulation. The coarser mesh can reduce amount of calculation but the result is not as accurate as finer mesh. Therefore, we need to select a suitable mesh that can achieve our requirements on both accuracy and running time.
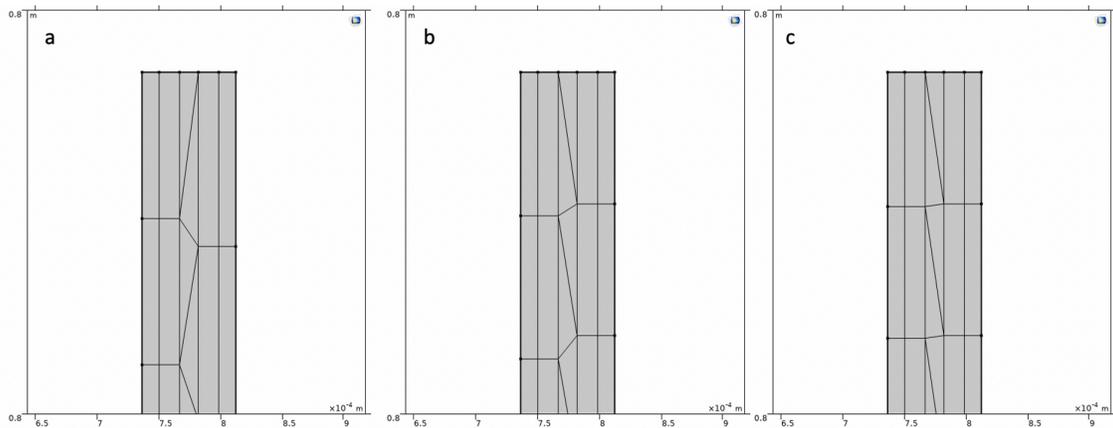
Figure 16. The mesh of our system at different levels of element size. (a) Extreme coarse element size. (b) Normal element size. (c) Extreme fine element size.

The mesh we used is normal, in order to know if it will influence the result too much, I ran the simulation at three different element sizes, extreme coarse, normal and extreme fine. Figure 17 shows the result that the element size won't influence the result in our system. The results in figure 17 are got at the same boundary conditions but different element sizes. The gas pressure in the inner tube is 200 kPa; the vacuum pressure is 15 inHg; the liquid flow rate is 0.009 ml/min.
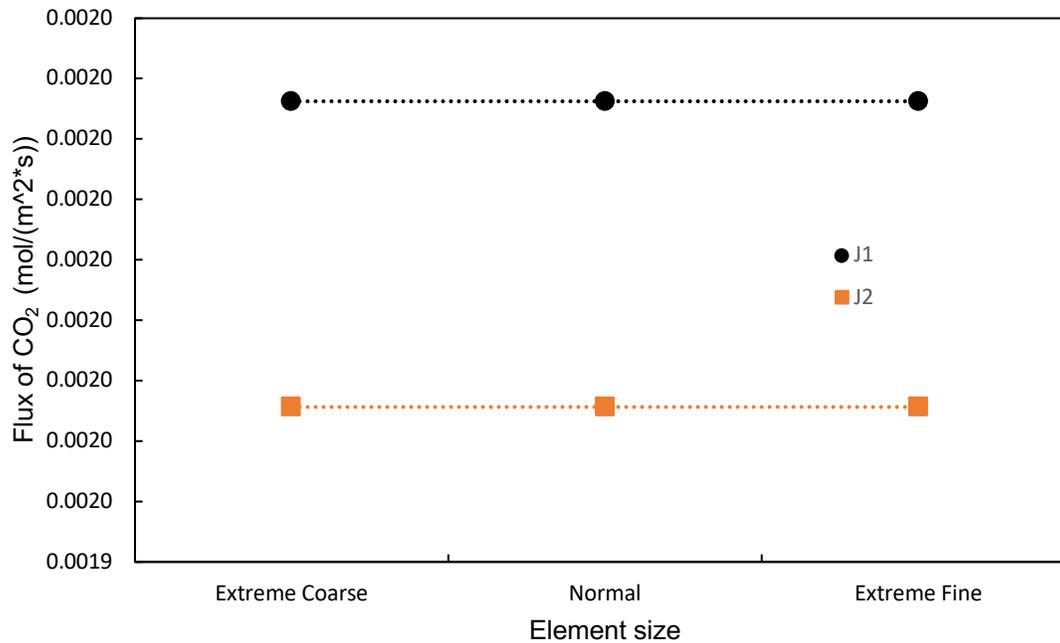
Figure 17. The flux of CO_2 at different element sizes from extremely coarse to extremely fine. J1 is the inlet flux of CO_2 from the inner tube permeates into the liquid. J2 is the flux of CO_2 from liquid goes into the outer tube.

3.7 Calculation of the Fraction of Recovered CO_2.

The major driver for CO_2/vacuum use in distributed systems is the ability to recapture and reuse it in a nearly closed system. In order to do the feasible analysis of CO_2 recovery, we use both experiments and simulation method to get the flux data of the system, which can be used to calculate the fraction of recovered CO_2.

For the flux of the separator, the inlet flux of CO_2 from the inner tube dissolves into water is the total flux (F_1[=] mmol/min) of the system. The flux of CO_2 which enters the vacuum phase in the outer tube is F_2, and the flux which leaves the system with the liquid flow is F_3. Therefore, $F_1 = F_2 + F_3$ and fraction of recovered CO_2 is equal to F_2/F_1.

For the simulation, we can get the value of F_1, F_2, and F_3 at different working conditions directly, then the fraction can be calculated easily by using F_2/F_1. However, we can only record

the data of F_1 in the experiments; the F_2 and F_3 can not be measured. Therefore, we use the F_1 at 0 ml/min liquid flow rate to calculate the F_2. When the liquid flow rate is 0 ml/min, which means no water enters and leaves the system, all CO_2 from the inner tube will goes into the outer tube, thus $F_1 = F_{2-0}$ at this point. From simulated data, we found the F_2 decreases as the liquid flow rate increases (Figure 18), by applying the percentage of the change of F_2 on experimental data, we got the F_2 of experimental data at different liquid flow rates.

For example, in the simulated data, the F_2 at 0.02 ml/min is 99% of the F_2 at 0 ml/min. Therefore, we can calculate the F_2 at 0.02 ml/min of experimental data by $F_{2-0} * 99\%$.
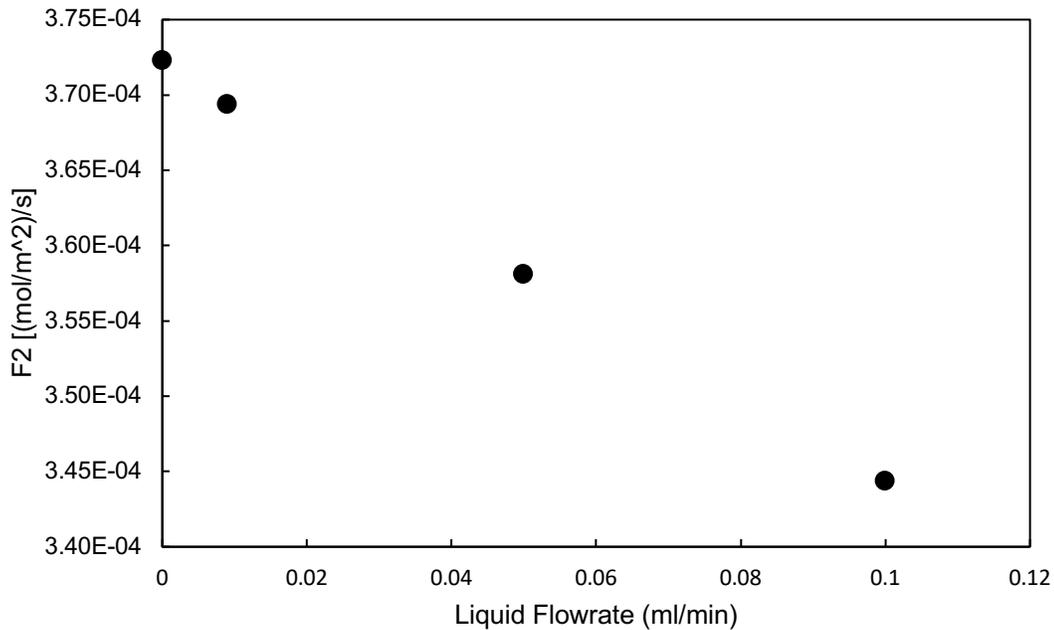
Figure 18. The simulated results of the flux of CO_2 entered the outer tube (F_2) as a function of liquid flowrate.

3.8 Experiments.

The system now is an auto-control system. We use LabVIEW 7.1 to control the equipment and collect data automatically. Three variables are critical for experiments control. We use these

three variables to control the purification performance of the system, they are gas pressure of CO_2, the liquid flow rate of water and the vacuum pressure of the outer tube,

3.8.1 Gas Pressure.

The CO_2 is in the inner tube and the pressure is controlled by the regulator on the gas tank, with a testable range of 100-250 kPa. Higher gas pressure can increase the diffusion and solubility of CO_2, more CO_2 dissolved into water will expand the concentration gradient of ion in water and make the purification performance of the system better.

3.8.2 Liquid Flow Rate.

Liquid flow rate corresponds to the residential time which means how long a unit of water will stay in the separator from the beginning to the end of the separator ($\tau = V_R / F$). Lower liquid flow rate(higher residence time) give particles more time to concentrate on the wall of the tube, and it also can make the performance of our system better. While the pumps can achieve substantially lower flowrates than used here (1 nL/min), we chose to operate between 0.001-0.1 mL/min such that steady-state ($\tau_{ss} \sim 3\tau$) could be achieved in less than 90 min. This was calculated based on an internal liquid dead volume, including the flow cell of 0.12 mL. Based on the work by Stone lab, diffusiophoreses typically induces velocities of 0.0033 mm/s which means 23 s would be needed to traverse the tubing gap of 0.086 mm.

3.8.3 Vacuum Pressure.

The vacuum phase in the outer tube has two main functions. One is increasing the flux of CO_2 through the water by lowering the downgradient pressure, which can let the system achieve better performance. The other function is recycling CO_2. In the future, our system will have a recycling system to recycle CO_2. A vacuum pump connects with outer tube to

collect CO_2 and then repump it into the system. Therefore, the system doesn't need to be replenished during the experiment.

4.0 Result.

4.1 Water Purification
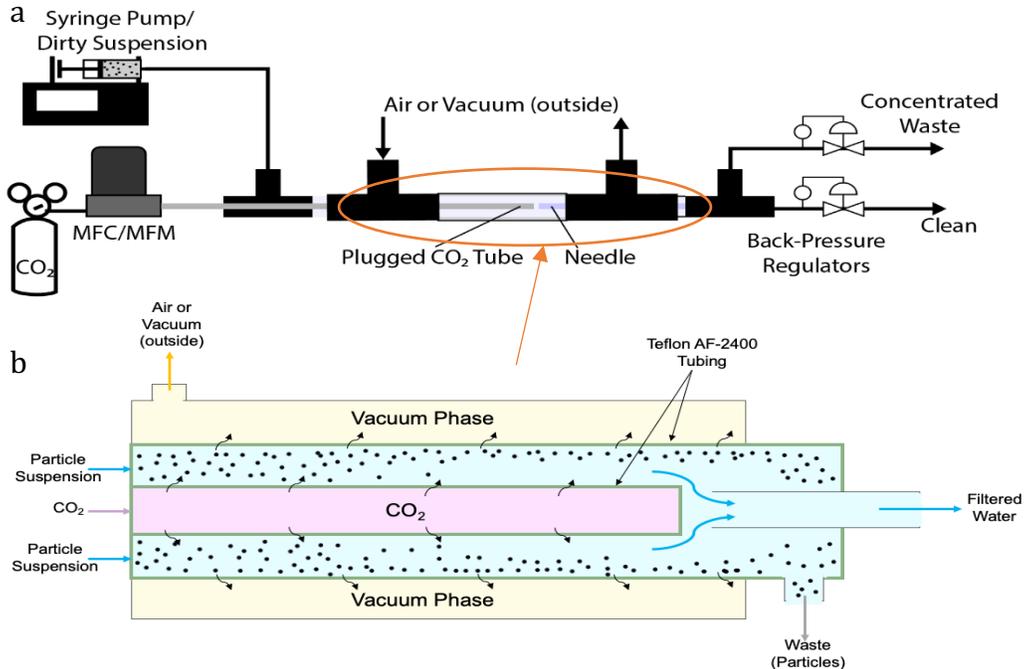
Figure 19. Membraneless water purification via diffusiophoresis. (a) Schematic of the water purification system. The particle suspension from syringe pump goes into the middle tube. The CO_2 from the gas tank flows through the mass flow controller into the inner tube. The vacuum pressure in the outer tube is controlled by a vacuum pump, which is connected with the outer tube. (b) Magnified image of the separator. The CO_2 from the inner tube permeates through Teflon AF-2400 tube into water then form a concentration gradient of ion in the water. The particles with negative surface charges migrate to the edge of the middle tube. Therefore, the filtered water can be gathered by a needle from the center of the middle tube. Partial CO_2 leaves the separator with water, and the rest of CO_2 goes into the vacuum phase.

The membraneless water purification is illustrated in the Figure 19a. Since most particles in nature have negative surface charge[13][14], the dirty suspension is made by polystyrene microspheres which have negative surface charge. The removal process of polystyrene particles using our separator is described in Figure 19b, the CO_2 permeates through the wall of the inner tube and dissolves into the flow stream, inducing the motion of particles which migrate to the wall of the middle tube by diffusiophoresis, thus the clean water can be collected by a needle from the

center of the middle tube, the turbidity of filtered water will be measured by UV spectrometer. In this system, several key factors have influence on the turbidity of filtered water. Therefore, we explored the influence of various factors on the result through experiments.

4.1.1 *Residence Time.*

Figure 20 shows the turbidity of filtered water and the fraction of removed particles at different residence time. The residence time corresponds to the liquid flow rate, it means how long the liquid takes from entering the separator to leaving the separator. It can be observed that the turbidity of filtered water is lower at high residence time. The slope of the curve is very steep at low residence time then becomes flatter at high residence time, that's because the particles need time to finish the migration process. Longer residence time will enable more particles to concentrate on the edge of the middle tube. However, after a certain residence time, most of the particles finished their migration process. Therefore, the slope of the curve flattens out.

Figure 20 also proves our assumption that our system can purify water. The initial turbidity of particle suspension is 243 NTU (Nephelometric Turbidity Unit), the turbidity of filtered water can reach 1.44 NTU and 99% particles are removed from particle suspension through the purification process. The WHO (World Health Organization) states the turbidity of drinking water should be lower than 5 NTU, and ideally lower than 1 NTU. The error bars in the plot are calculated by standard deviation of five sets of data.
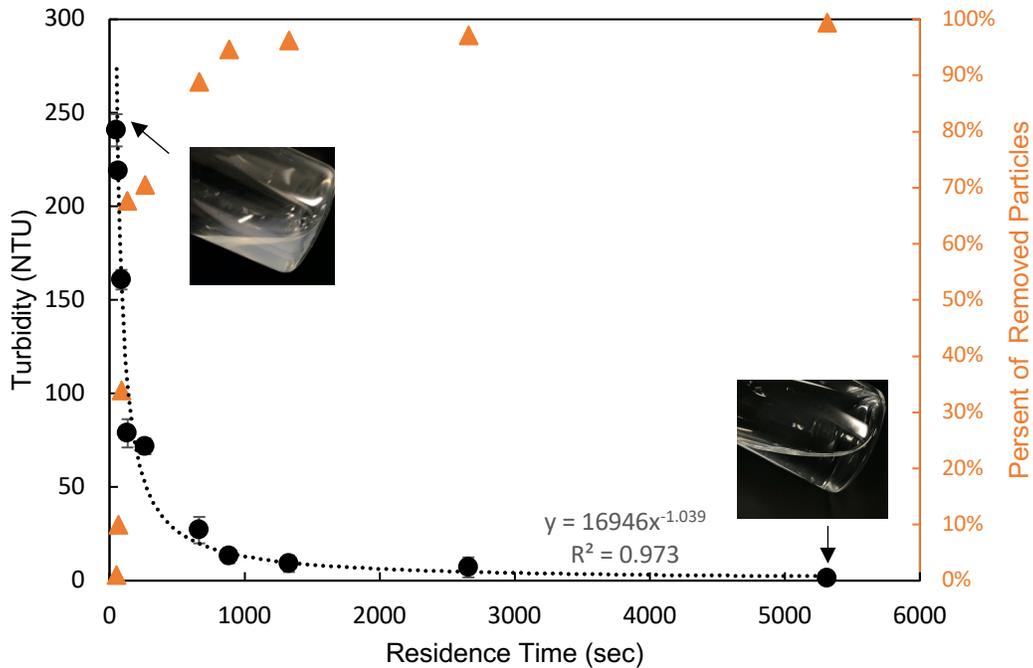
Figure 20. The turbidity of filtered water as a function of residence time (black). The fraction of removed particles as a function of residence time (orange). The gas pressure of CO_2 is 200kPa, and vacuum pressure is 15inHg. The initial turbidity of particle suspension is 243NTU.

4.1.2 Gas Pressure and Vacuum Pressure

The influence of gas pressure of CO_2 on the turbidity of filtered water can be observed in figure 21. Increasing gas pressure can reduce the turbidity of filtered water at the same vacuum pressure, residence time, etc. Since higher gas pressure will cause a higher concentration of CO_2 in the water, then the concentration gradient of ion is larger than lower gas pressure. Therefore, the motion speed of particles in the water will be faster; thus more particles can be concentrated at the wall of the middle tube while other working conditions remain the same.

At the same time, the influence of vacuum pressure in the outer tube can also be observed in figure 21 and figure 22. The turbidity of filtered water goes down after applying vacuum pressure in the outer tube. The vacuum pressure will reduce the concentration of CO_2 in the water at the edge of the middle tube. However, the concentration at the edge of the inner tube doesn't

change since the gas pressure in the inner tube is constant. Therefore, the concentration gradient of ion is increased by raising the vacuum, which has the same function as raising the gas pressure of CO_2.
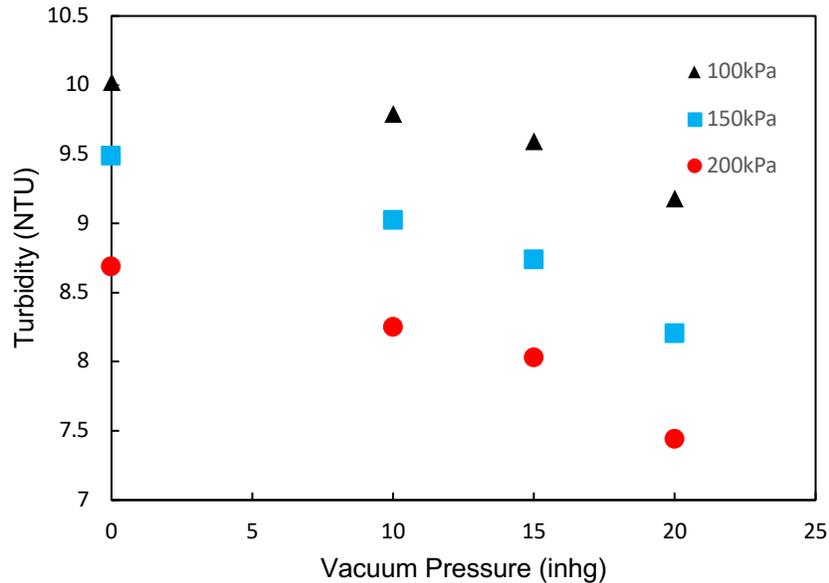
Figure 21. The turbidity of filtered water as a function of vacuum pressure in the outer tube for the family of gas pressure of CO_2. The residence time is constant at the 70s. The initial turbidity of dirty suspension is 16 NTU.
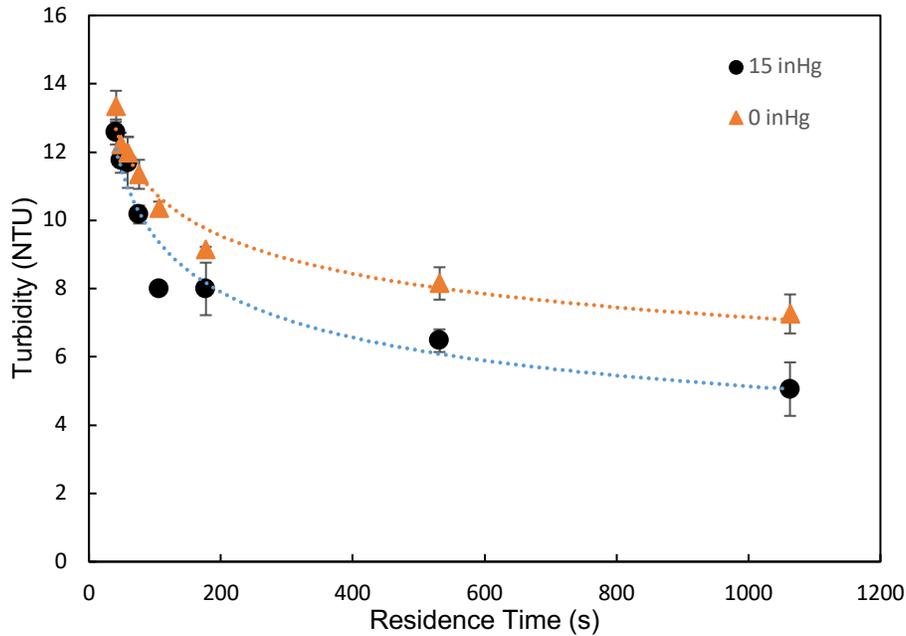
Figure 22. The turbidity of filtered water at different residence times for the family of vacuum pressure in the outer tube. The gas pressure of CO_2 is 200kPa. The initial turbidity of particle suspension is 19NTU.

4.1.3 Needle Distance

Another variable that can be controlled is the distance of the gap between the end of the inner tube and the needle. At the end of the inner tube, the particles are concentrated at the edge of the middle tube, and the clean water will enter the needle. However, some particles will enter the needle if the gap is too big, like the figure 23a. This assumption is supported by the data in figure 24. In this experiment, we pulled the needle out 1 mm each time to observe the change of the turbidity of the filtered water. The residence time is constant at 70 s, the gas pressure of the inner tube is 200 kPa and the vacuum pressure in the outer tube is 15 inHg. From the data of figure 24, we can see the increase in turbidity of filtered water is accompanied by an increase in the distance of the gap in the first half of the data set. After 5 mm, the turbidity doesn't raise up, that's because the particles and the clean water are completely mixed at that position.
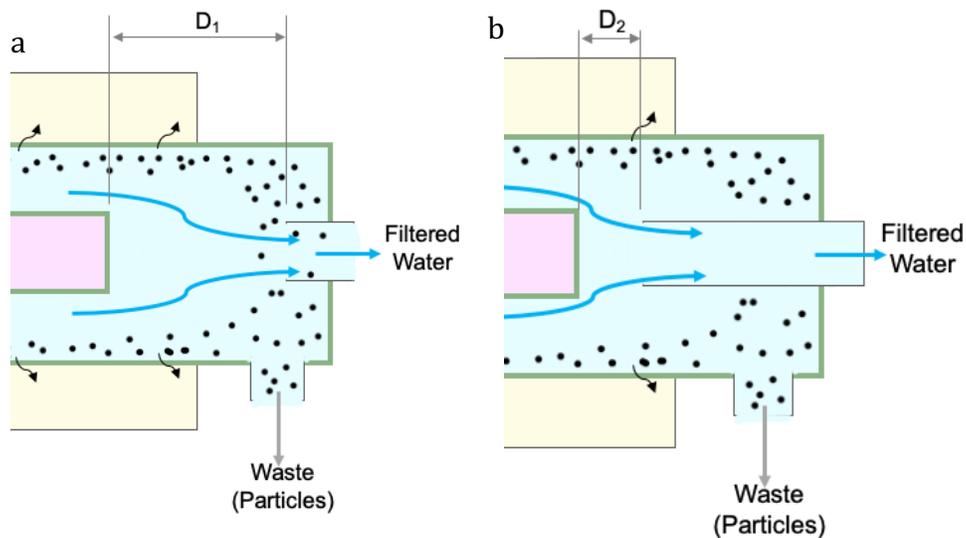
Figure 23. The schematics of the change of the distance of the gap between the end of the inner tube and the needle. (a)(b) The motion of particles at different distance of the gap, D1>D2. More particles will enter the needle by increasing the distance of the gap.
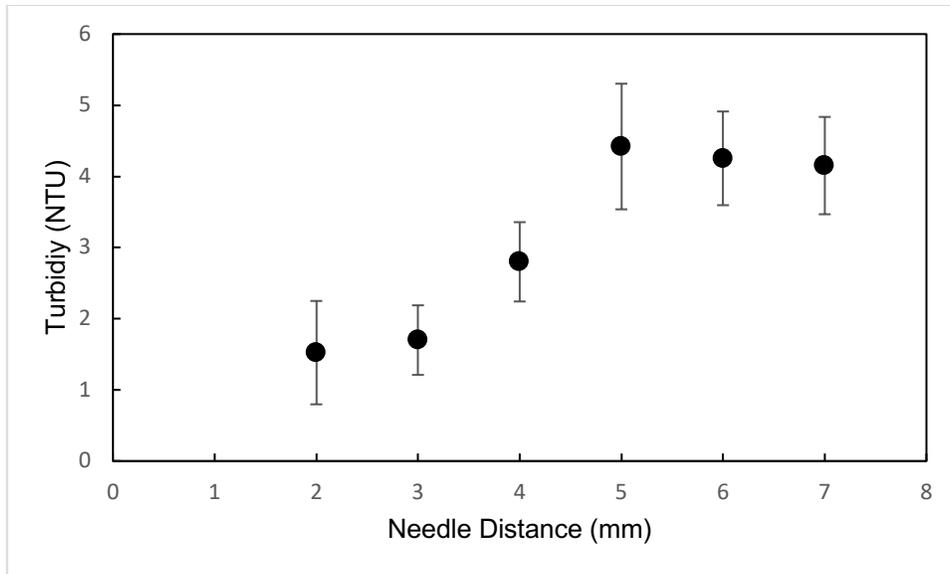
Figure 24. The turbidity of filtered water as a function of the distance between the end of the inner tube and the needle. The initial turbidity of dirty suspension is 7 NTU.

4.2 Feasible Analysis of CO_2 Recovery

The final goal of our project is to construct a water purification system that only needs electricity to operate. So as to achieve this target, the CO_2 needs to be recycled, that is one reason why our system needs an outer tube which is connected with a vacuum pump, it's used to collect the CO_2. In order to verify the feasibility of our idea, we ran the system at different conditions and recorded the gas flow rate of CO_2, and then we can calculate what percentage of CO_2 permeates into the outer tube. Therefore, we use COMSOL to simulate the system to determine the theoretical flux of CO_2 into the system.

4.2.1 Concentration Profile
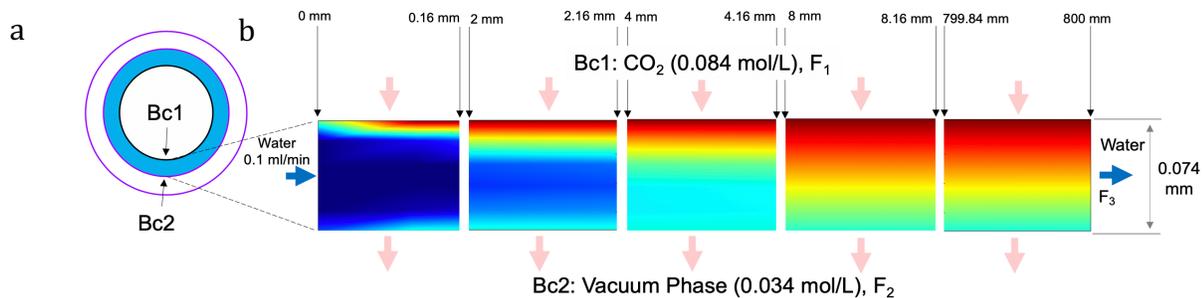
Figure 25. Concentration distribution of CO_2 in the separator. The length of the separator is 0.8m. The color from red to blue corresponds to the concentration of CO_2 from high to zero. The liquid enters the separator from the left side and leaves the system from the right side. The CO_2 from the inner tube dissolves into the liquid from the top, and the bottom is the vacuum phase in the outer tube. (a) Cross-section of tube-in-tube-in-tube separator. (b) shows the concentration distribution at different position of the separator,

Figure 25 shows the concentration distribution of CO_2 in the liquid layer of separator. The CO_2 dissolves into the water from both the inner tube and the outer tube at the very beginning of the separator, that's because even the outer tube is connected with a vacuum pump which can apply vacuum pressure in the outer tube, but the outer tube isn't pure vacuum. Therefore, the CO_2 in the outer tube will also dissolve into the liquid layer. After the first 8 mm the system reaches the

steady-state, partial CO_2 in the water will permeate into the vacuum and the rest of CO_2 will leave the water with liquid flow.

In figure 25, F_1 is the inlet flux of CO_2 from the inner tube dissolves into the liquid. F_2 is the flux of CO_2 from liquid goes into the vacuum phase in the outer tube. F_3 is the flux of CO_2 leaves the separator with liquid flow. Therefore, $F_1=F_2+F_3$.

4.2.2   Flux Profile

Figure 26 and 27 show the influence of different variables on the total flux (F_1) of CO_2 in the system. The F_1 is the inlet flux of CO_2 from the inner tube into the liquid layer. During this process, three variables can be controlled, gas pressure of the inner tube, vacuum pressure of the outer tube and residence time. The residence time from 44 sec to ∞ seconds corresponds to the liquid flow rate from 0.1 ml/min to 0 ml/min.

In figure 26, the gas pressure of the inner tube has a certain effect on the F_1 in both experimental data and simulated data. However, the residence time has a very limited effect on the F_2.
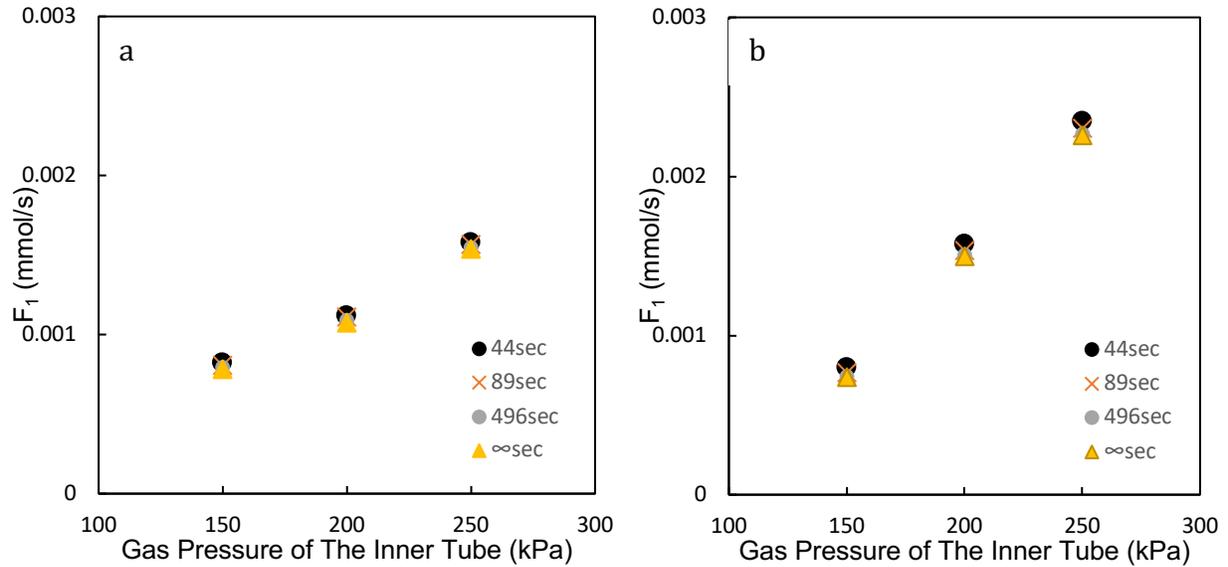
Figure 26. The total flux (F_1) of CO_2 from the inner tube as a function of gas pressure in the inner tube (150 kPa – 250 kPa) for the family of residence time (44 s - ∞ s). The vacuum pressure in the outer tube is 0 inHg. (a) Experimental data of CO_2 inlet flux. (b) Simulated data of CO_2 inlet flux.

The influence of the vacuum pressure of the outer tube can be observed in figure 27, that increasing vacuum pressure can raise the F_1. By comparing the effect of these three variables, we can know the gas pressure of CO_2 in the inner tube has the greatest influence on the F_1, then the vacuum pressure in the outer tube. The residence time basically has very less effect on the F_1.
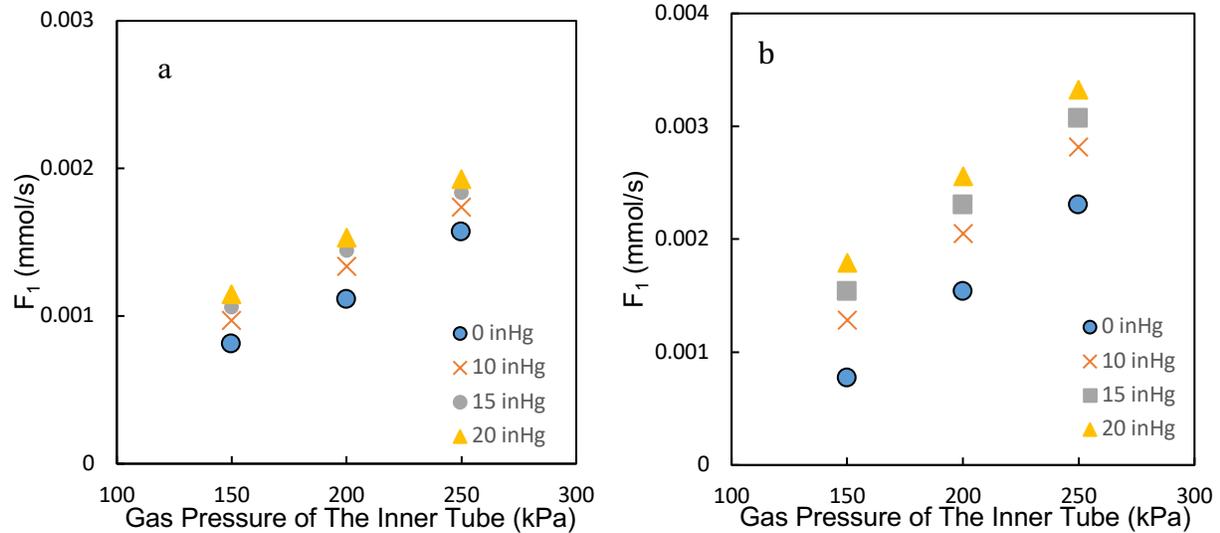
Figure 27. The total flux (F_1) of CO_2 from the inner tube as a function of gas pressure in the inner tube for the family of vacuum pressure in the outer tube (0 - 20 inHg). The residential time of liquid is constant at 89 seconds. (a) Experimental data of CO_2 inlet flux. (b) Simulated data of CO_2 inlet flux.

4.2.3   Fraction Recovered

Another function of the outer tube is using vacuum pressure to collect CO_2 and recycle it. The fraction of recovered CO_2 is equal to F_2/F_1, where F_1 is the inlet flux of CO_2 from the inner tube dissolving into the liquid layer, F_2 is the flux of CO_2 entering the vacuum phase. Figure 28 and 29 exhibit the fraction of recovered CO_2 at different working conditions. In figure 28, both residence time and gas pressure of the inner tube can generate the effect on the fraction. For the residence time, higher residence time corresponds to the lower liquid flow rate. Lower liquid flow rate means less CO_2 will leave the system by liquid flow and more CO_2 will be recovered by vacuum phase. Increasing the gas pressure of the inner tube can also raise the fraction at the same residence time, because the pressure gradient between the inner tube and the outer tube is expanded by increasing gas pressure.
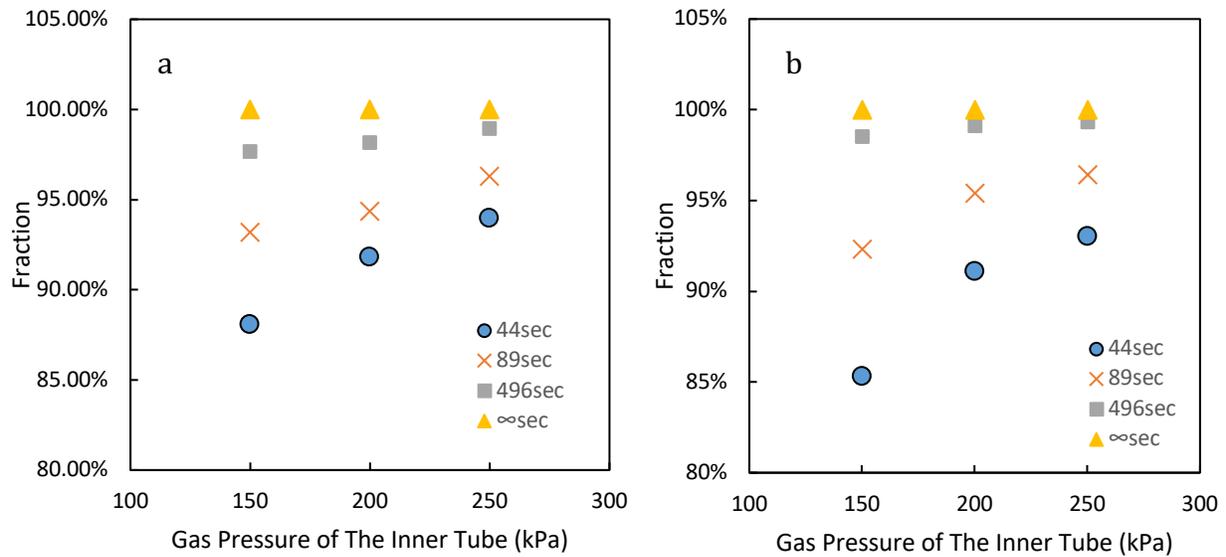
Figure 28. The fraction of recovered CO_2 as a function of gas pressure in the inner tube (150 – 250 kPa) for the family of residential time (44 - ∞ sec). (a) Experimental data. (b) Simulated data.

The vacuum pressure in the outer tube is another factor that has an influence on the fraction of recovered CO_2. Changing vacuum pressure has the same effect as increasing gas pressure in the inner tube. They all amplify the pressure gradient between the inner tube and the outer tube, which causes more CO_2 to permeate through the liquid layer into the vacuum phase. In figure 29, the turbidity of filtered water at 15 inHg vacuum pressure is lower than the turbidity at 0 inHg,

In order to get a high fraction of recovered CO_2 to recycle the CO_2, we need to use a low liquid flow rate, a high gas pressure of the inner tube and high vacuum pressure in the outer tube.
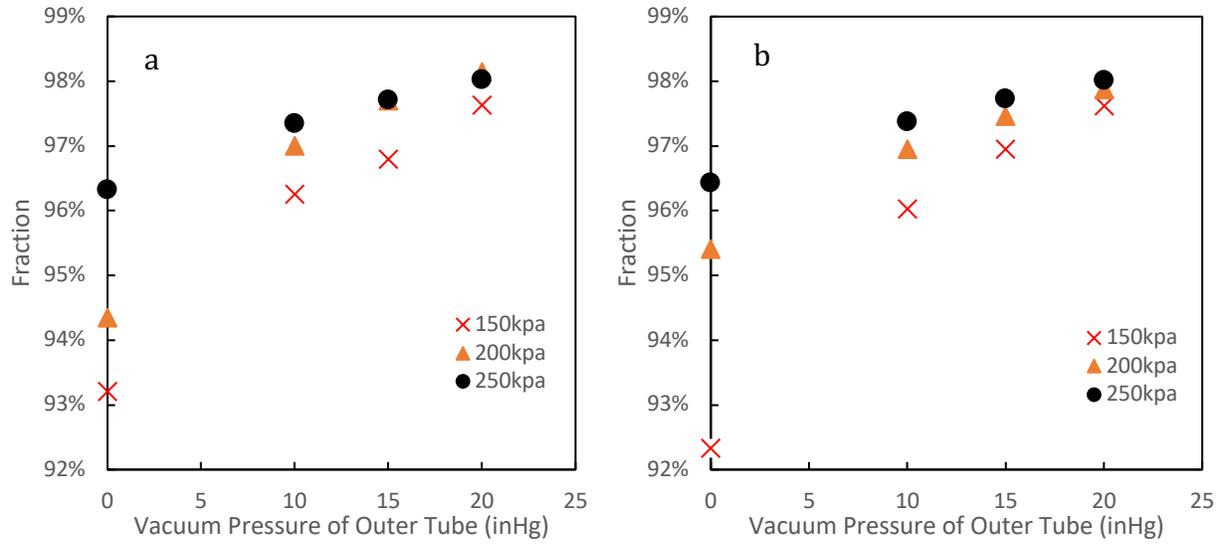
Figure 29. The fraction of recovered CO_2 as a function of vacuum pressure in the outer tube (0 – 20 inHg). (a) Experimental data. (b) Simulated data.

5.0 Conclusion

In this study, we present a membraneless water purification system which uses a tube-in-tube-in-tube separator to remove particles from dirty water. The performance of the system is tested by changing the working conditions, such as different liquid flow rate, gas pressure and vacuum pressure. The result shows our system can purify the dirty water (243 NTU) to 1.44 NTU, which is in the range of drinking water standard. The primary goal of our project is to design and construct a water treatment system which only needs electricity to operate. Therefore, we analyzed the feasibility of CO_2 recovery by both experimental method and software simulation method. The result shows more than 98% of CO_2 can be recycled at certain working conditions.

For the water purification, the turbidity of filtered water is controlled by the liquid flow rate, the gas pressure of the inner tube and the vacuum pressure of the outer tube. The liquid flow rate corresponds to the residence time of the liquid in the separator. Lower liquid flow rate gives particles more time to migrate to the edge of the middle tube, then the turbidity of filtered water is reduced. The gas pressure and vacuum pressure have the same function on the system. Increasing both of them will expand the pressure gradient between the inner tube and the outer tube, which will cause more CO_2 dissolved into water then further increase the concentration gradient of ion and increase the migration speed of the particles. Therefore, in order to get low turbidity filtered water, we need to use a low liquid flow rate and high gas pressure and vacuum pressure.

The other function of the outer tube is recycling CO_2. After the CO_2 from the inner tube dissolves into water, partial CO_2 will saturate in the water and leave the system by liquid flow; the rest of CO_2 will desorb from water at the boundary between the liquid layer and vacuum phase and be recycled by vacuum phase. In this process, a higher liquid flow rate will carry more CO_2 to leave the system and reduce the fraction of recovered CO_2. However, increasing gas pressure and

vacuum pressure will amplify the pressure gradient between the inner tube and the outer tube, which will cause more CO_2 to permeate through the liquid layer into the vacuum phase. Therefore, decreasing liquid flow rate and raising gas pressure and vacuum pressure can increase the fraction of recovered CO_2.

However, our system has some limitations. The first one is tube fouling. Some particles will stick on the wall of Teflon tube after long time running and influence the diffusion rate of CO_2. The second one is the surface charge of contaminants. The current system can only remove contaminants with negative surface charge from water, but the real water system has a lot of unknown contaminants, we need to consider how to remove the particles with different surface charge. The third one is the pH of the filtered water. Our separator will form a concentration gradient of H^+ in the water layer that causes the pH value of filtered water lower than the regular water. Ph value has a very important effect on water quality. Different pH values will cause some pollutants in the water to form or decompose, causing harm to human beings or aquatic animals.

6.0 Recommendations for Future Work.

From a scientific perspective, substantial work is needed to prove the diffusiophoretic force acting on particles. Optimization and characterization should be performed to elucidate the effect of several factors.

The first one is diffusiophoretic path length, which is the thickness of the gap between the inner tube and the outer tube. The path length will influence the concentration distribution of ion in the water and further influence the moving speed of particles. At the same time, longer path length will increase the minimal residence time of particle suspension, because the particles need more time to finish the migration.

Particle loading, size and surface charge also need to be considered. These characteristics of particles control the performance of particles in the water. For example, the migration direction of positive charged particles and negative charged particles are opposite.

Another one is the ability to separate other charged or slightly charged species, such as heavy metals, PFAS, bacteria, etc. In real dirty water supplies, many substances in water are considered as water pollutants and divided into several categories, such as pathogens, inorganic contaminants, anions and cations and water-soluble radioactive substances. All these contaminants will cause health problems in humans and other organisms in the ecosystem. Bacteriological contamination acts as disease causing germs and pathogens. Trace elements and heavy metals are delivered into surface water and groundwater by human activities, such as industrial wastes and agricultural chemicals. Most of these contaminants are considered critical for the health of human and living organisms. Cations like sodium (Na^+), potassium (K^+), magnesium (Mg^{+2}) and anions including nitrates (NO_3^-), nitrites (NO_2^-), chlorides (Cl^-), etc. These ions are important for processes in the human body. However, these ions may make the water unfit for living organisms

if the concentrations are too high[3]. pH value will also affect the quality of water. For example, Too low PH can cause S_2^-, CN^- to change to H_2S, HCN, they are toxicity. If the pH value is too high, NH_4^+ will change to NH_3, which can corrode fish and shrimp gill tissue and make it difficult to breathe. Therefore, how to control the concentration of other species in water should be considered in the future work, such as bacteria, heavy metal, pH value, etc.

In order to get a more accurate simulated result, we need to further optimize the system in the COMSOL. At the current stage, we only simulated the diffusion of the CO_2-Water system. However, CO_2 can form several different species in the water, such as $(CO_3^{2-},\ HCO_3^-, H^+)$, and they have their own diffusion performance in the water. In the future work, we should add these species in the simulated system. The motion of particles should also be tracked in the COMSOL to get theoretical result of particle separation. The mesh of the current model is built by the software automatically, but the difference between extremely coarse and extremely fine is not obvious. In the future, we need to define the mesh manually to get finer mesh.

From a manufacturability and technology transfer perspective, here are two factors which should be focused on. One is the tubing fouling by particle accumulation. After a long-running time of the system, some particles will stick to the wall of the tube and affect the purification performance.

The other one is expanding the production of the system. Currently, even the turbidity of filtered water can reach the drinking water standard, but the production is too low. Therefore, we need to amplify the production based on the current system.

References

[1] P. H. Gleick, "Water and Conflict: Fresh Water Resources and International Security," *Int. Secur.*, vol. 18, no. 1, p. 79, 1993, doi: 10.2307/2539033.

[2] I. A. Shiklomanov, "Appraisal and Assessment of world water resources," *Water Int.*, vol. 25, no. 1, pp. 11–32, 2000, doi: 10.1080/02508060008686794.

[3] A. Azizullah, M. N. K. Khattak, P. Richter, and D. P. Häder, "Water pollution in Pakistan and its impact on public health - A review," *Environ. Int.*, vol. 37, no. 2, pp. 479–497, 2011, doi: 10.1016/j.envint.2010.10.007.

[4] VITO-SCT Revision of Technical Notes, "Ultrafiltration - EMIS." 2008.

[5] G. Owen, M. Bandi, J. A. Howell, and S. J. Churchouse, "Economic assessment of membrane processes for water and waste water treatment," *J. Memb. Sci.*, vol. 102, no. C, pp. 77–91, 1995, doi: 10.1016/0376-7388(94)00261-V.

[6] Greenwood, *Chemistry of the Elements*. Elsevier Science & Technology Books, 1996.

[7] A. Fick, "Ueber Diffusion," *Ann. Phys.*, vol. 170, no. 1, pp. 59–86, Jan. 1855, doi: 10.1002/andp.18551700105.

[8] C. P. Society., "Transactions of the Cambridge Philosophical Society.," *Transactions of the Cambridge Philosophical Society.* [University Press], [Cambridge], 1822.

[9] S. Shin, O. Shardt, P. B. Warren, and H. A. Stone, "Membraneless water filtration using CO_2," *Nat. Commun.*, vol. 8, no. May, pp. 1–6, 2017, doi: 10.1038/ncomms15181.

[10] J. Zhang, A. R. Teixeira, H. Zhang, and K. F. Jensen, "Automated in Situ Measurement of Gas Solubility in Liquids with a Simple Tube-in-Tube Reactor," *Anal. Chem.*, vol. 89, no. 16, pp. 8524–8530, 2017, doi: 10.1021/acs.analchem.7b02264.

[11] M. O'Brien, "An automated colorimetric inline titration of CO_2 concentrations in solvent flow streams using a Teflon AF-2400 tube-in-tube device," *J. CO2 Util.*, vol. 21acsac, no. September, pp. 580–588, 2017, doi: 10.1016/j.jcou.2017.08.020.

[12] J. Zhang, A. R. Teixeira, H. Zhang, and K. F. Jensen, "Flow toolkit for measuring gas diffusivity in liquids," *Anal. Chem.*, vol. 91, no. 6, pp. 4004–4009, 2019, doi: 10.1021/acs.analchem.8b05396.

[13] R. Beckett and N. P. Le, "The role or organic matter and ionic composition in determining the surface charge of suspended particles in natural waters," *Colloids and Surfaces*, vol. 44, no. C, pp. 35–49, 1990, doi: 10.1016/0166-6622(90)80185-7.

[14] 2016) (Nurarif & Kusuma, "The surface charge of suspended particles in estuarine and coastal waters K.," *J. Chem. Inf. Model.*, vol. 53, no. 9, pp. 1689–1699, 2013, doi: 10.1017/CBO9781107415324.004.

[15] K. A. Hunter and P. S. Liss, "Organic matter and the surface charge of suspended particles in estuarine waters," *Limnology and Oceanography*, vol. 27, no. 2. pp. 322–335, 1982, doi: 10.4319/lo.1982.27.2.0322.

[16] A. This, "Turbidity, nephelometric," vol. 85, pp. 5–6.

[17] T. E. of E. Britannica, "Colloid," *Encyclopædia Britannica, inc.* [Online]. Available: https://www.britannica.com/science/colloid.

[18] R. Beckett, G. Nicholson, B. T. Hart, M. Hansen, and J. Calvin Giddings, "Separation and size characterization of colloidal particles in river water by sedimentation field-flow fractionation," *Water Res.*, vol. 22, no. 12, pp. 1535–1545, 1988, doi: 10.1016/0043-1354(88)90166-2.

[19] U. Alonso, T. Missana, A. Patelli, and V. Rigato, "Bentonite colloid diffusion through

the host rock of a deep geological repository," *Phys. Chem. Earth*, vol. 32, no. 1–7, pp. 469–476, 2007, doi: 10.1016/j.pce.2006.04.021.

[20]   F. H. Frimmel, F. Von Der Kammer, and H. C. Flemming, "Colloidal transport in porous media," *Colloidal Transport in Porous Media*. pp. 1–291, 2007, doi: 10.1007/978-3-540-71339-5.

[21]   R. Voegelin, A.; Kretzschmar, "Stability and mobility of colloids in Opalinus Clay," *Technischer Bericht*. Nagra., Wettingen, 2009.

[22]   L. Yang and K. F. Jensen, "Mass transport and reactions in the tube-in-tube reactor," *Org. Process Res. Dev.*, vol. 17, no. 6, pp. 927–933, 2013, doi: 10.1021/op400085a.

[23]   I. Pinnau and L. G. Toy, "Gas and vapor transport properties of amorphous perfluorinated copolymer membranes based on 2,2-bistrifluoromethyl-4,5-difluoro-1,3-dioxole/tetrafluoroethylene," *J. Memb. Sci.*, vol. 109, no. 1, pp. 125–133, 1996, doi: 10.1016/0376-7388(95)00193-X.

[24]   R. Sander, "Compilation of Henry's law constants (version 4.0) for water as solvent," *Atmos. Chem. Phys.*, vol. 15, no. 8, pp. 4399–4981, 2015, doi: 10.5194/acp-15-4399-2015.

[25]   D. W. Mueller, "An introduction to the finite element method using MATLAB," *Int. J. Mech. Eng. Educ.*, vol. 33, no. 3, pp. 260–277, 2005, doi: 10.7227/IJMEE.33.3.8.

Appendix A

Supporting Information

A.1 UV Spectrum.

Figure A.1 is the UV spectrum of filtered water we got from UV spectrum. After we got the spectrum, we recorded the value of each peak of the spectrum. By comparing the value of each peak, we found the peak at 645 nm wavelength is more stable than others. Therefore, we calculated the turbidity of filtered water based on the value of the peak at 645 nm wavelength.
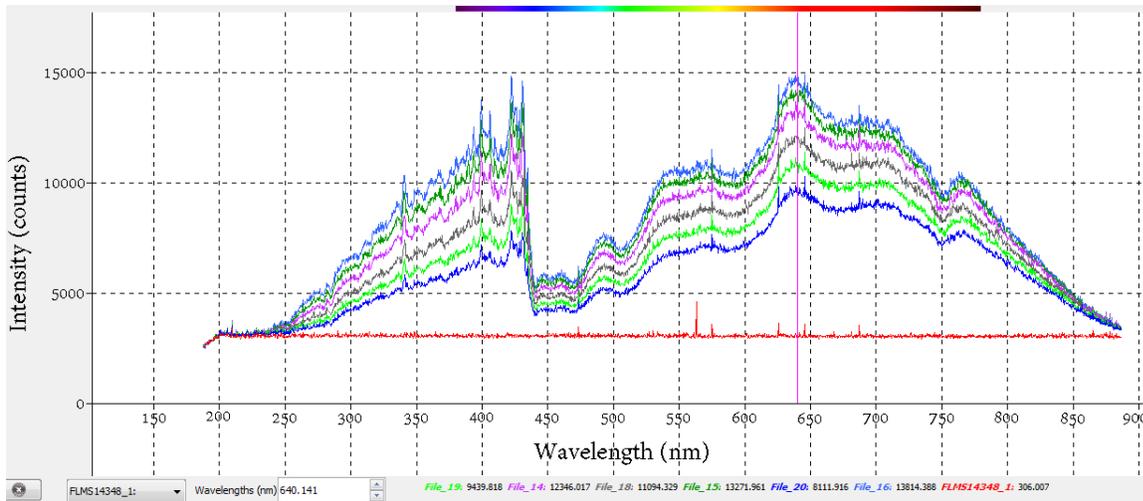
Figure A.1: UV spectrum of the filtered water.

A.2 Bacteria Separation

We did bacteria separation once in our previous shorter separator. The bacteria we used is E.coli from Prof Steward's lab. In the figure A.2, the relative concentration of bacteria was reduced from 0.46 to 0.25, 45% bacteria was removed. Even the result is not perfect, that because the separator length and working condition is not as good as current system, but the result shows our system can separates bacteria from liquid.
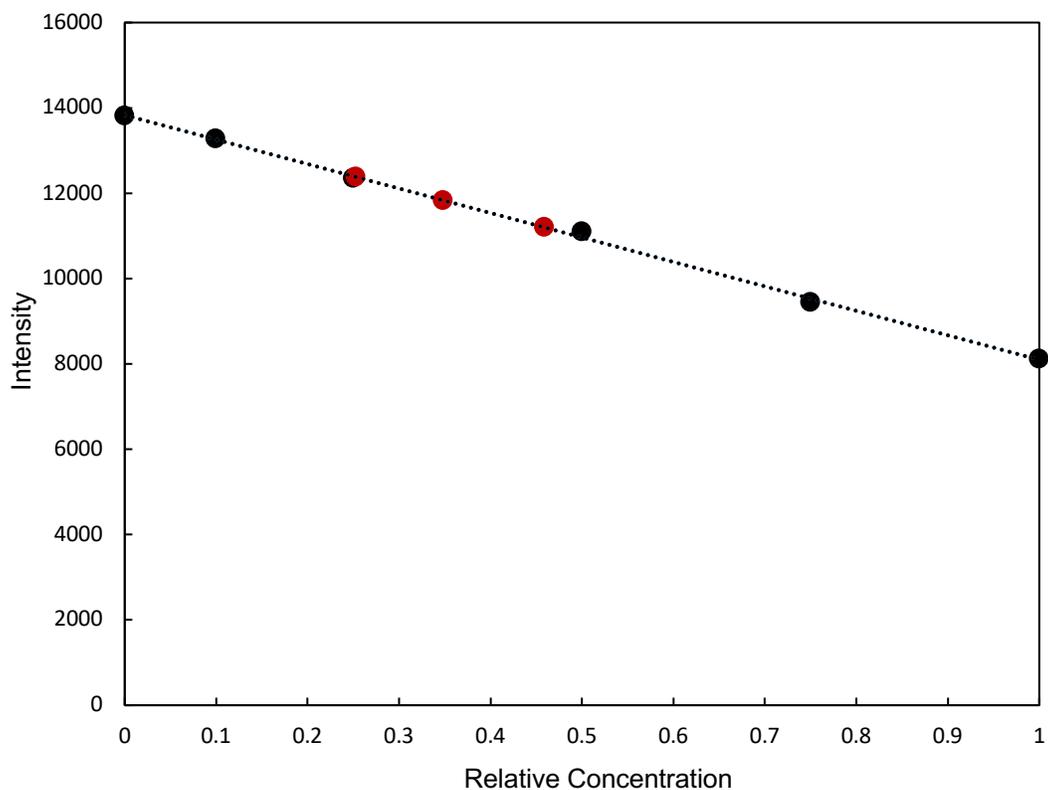
Figure A.2: The intensity of filtered water as a function of Relative concentration of the sample. The black points are calibration curve. The red points are the concentration change of bacteria.

A.3 Raw Data of Particle Separation

In the particle separation experiments, we recorded the intensity of filtered water five times at each working condition, such as different liquid flowrate, different gas pressure in the inner tube, and different vacuum pressure in the outer tube. Then took the average value of the five numbers.
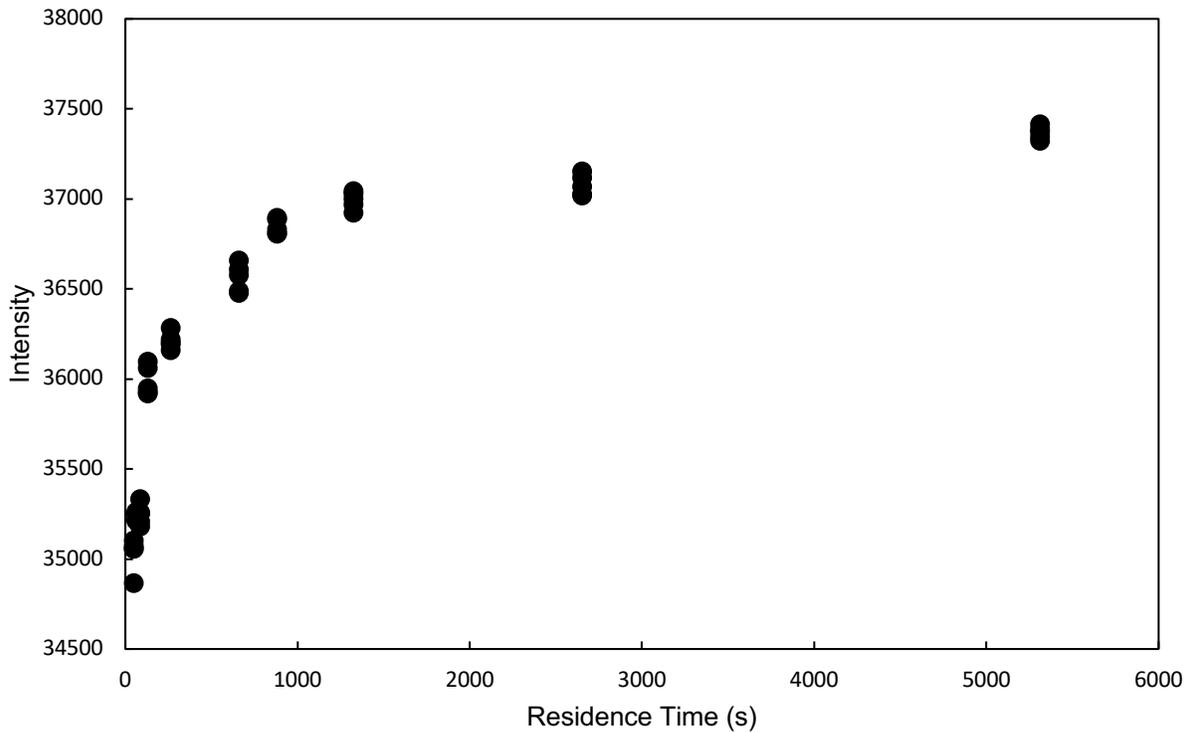
Figure A.3 The intensity of filtered water as a function of residence time
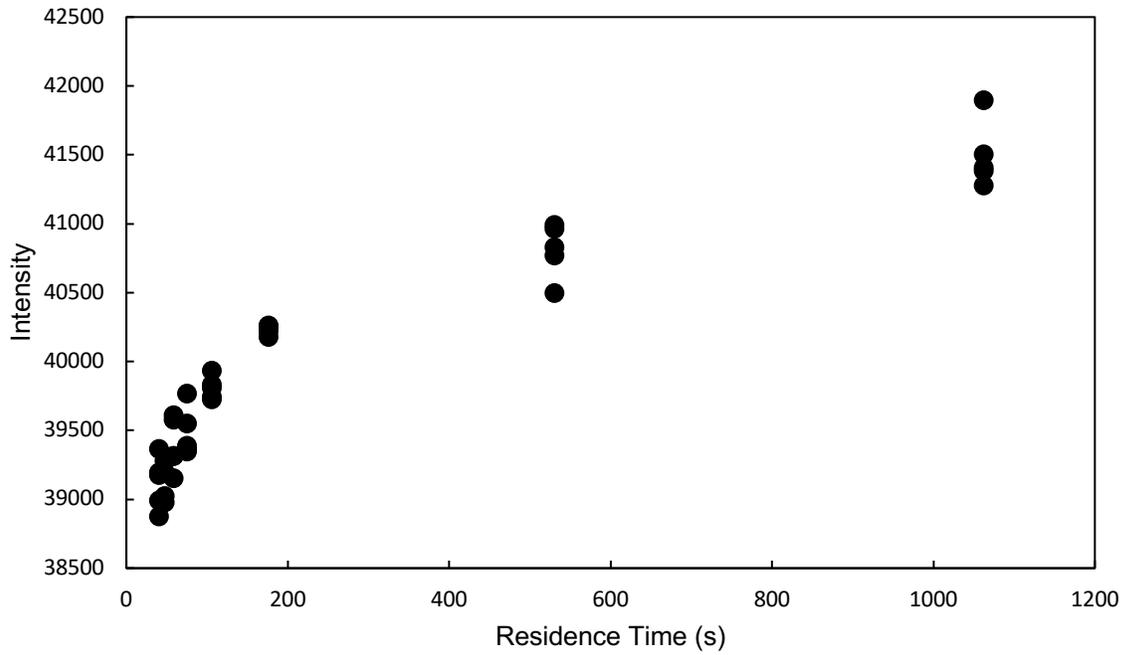
Figure A.4: The intensity of filtered water as a function of residence time. The vacuum pressure is 0 inHg.
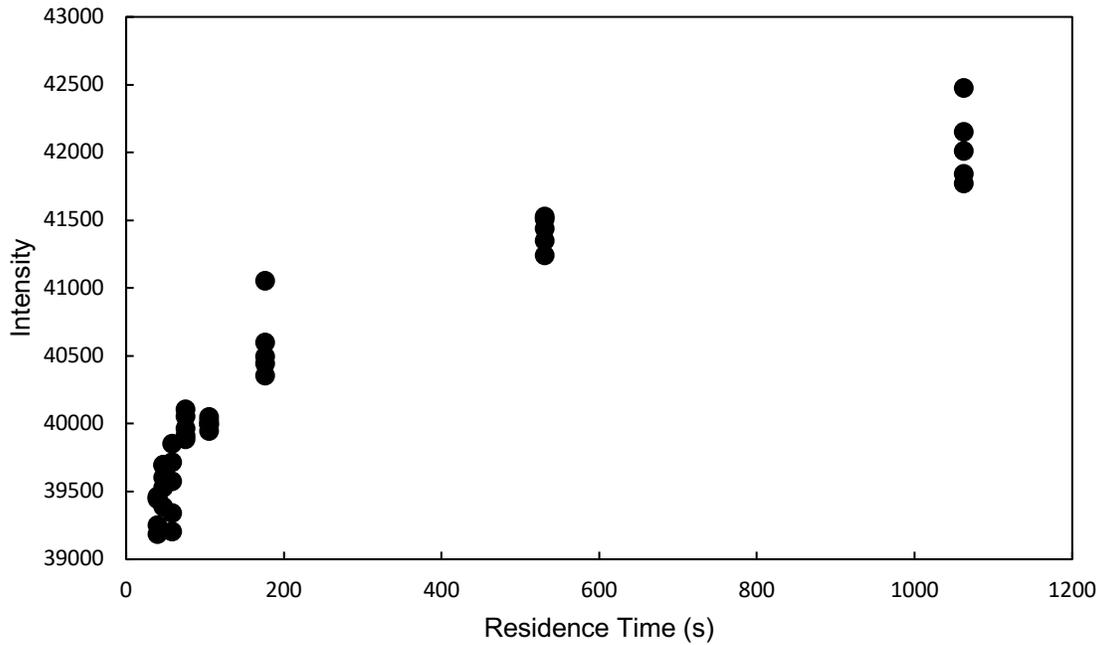
Figure A.5: The intensity of filtered water as a function of residence time. The vacuum pressure is 15 inHg.
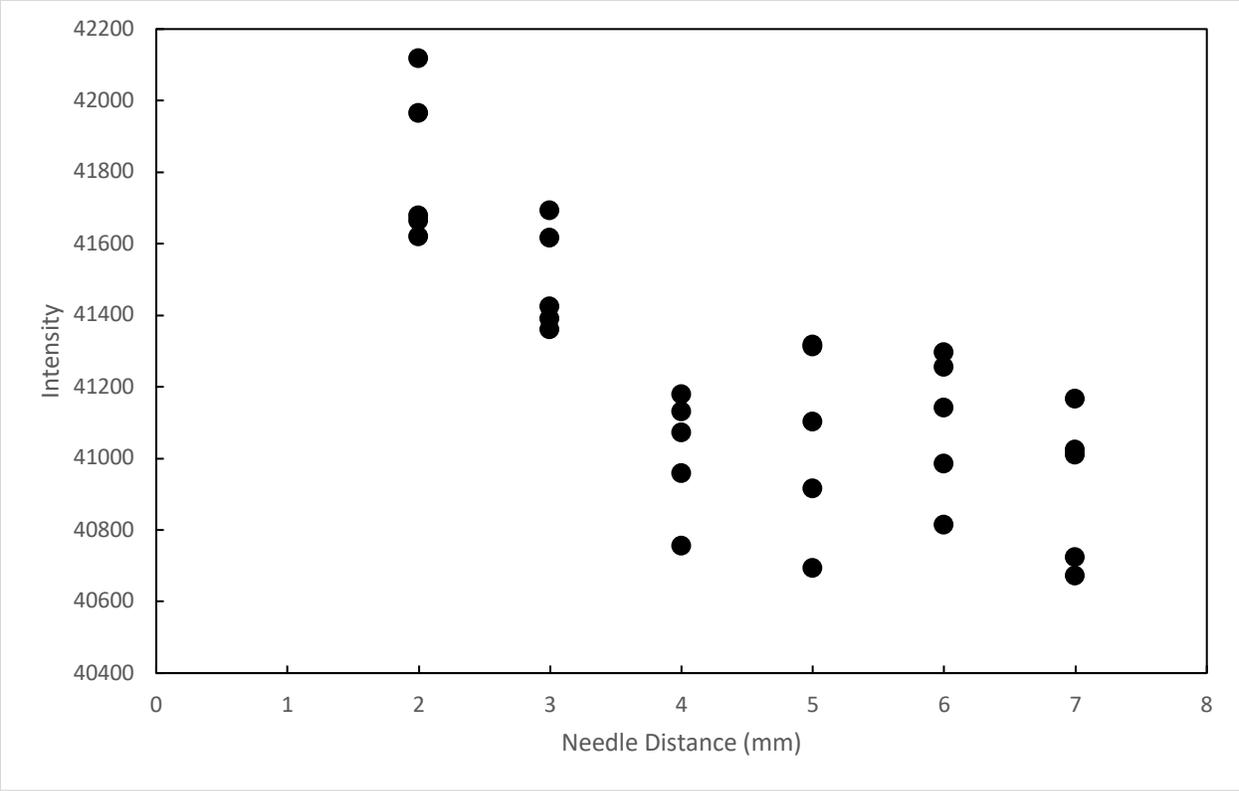
Figure A.6: The intensity of filtered water as a function of needle distance.

A.4 CO_2 Recovery.

Simulated data. The raw data of the inlet flux(J_1) of CO_2 and the flux of CO_2 entered the outer tube (J_2) are showed in the tables (Table A.1-A-6). The unit of flux is (mol/(m^2*s)

Table A.1: The simulated inlet flux of CO_2 (J_1) at different vacuum pressure. Gas pressure is 150 kPa

Liquid Flow rate(ml/min)	0 inHg	10 inHg	15 inHg	20 inHg
0.1	0.00043	0.00071	0.00084	0.00098
0.05	0.00042	0.00069	0.00083	0.00097
0.009	0.00040	0.00068	0.00082	0.00096
0	0.00040	0.00068	0.00082	0.00096

Table A.2: The simulated inlet flux of CO_2 (J_1) at different vacuum pressure. Gas pressure is 200 kPa

Liquid Flow rate(ml/min)	0 inHg	10 inHg	15 inHg	20 inHg
0.1	0.00085	0.00112	0.00126	0.00140
0.05	0.00083	0.00111	0.00124	0.00138
0.009	0.00081	0.00109	0.00123	0.00137
0	0.00081	0.00109	0.00123	0.00137

Table A.3: The simulated inlet flux of CO_2 (J_1) at different vacuum pressure. Gas pressure is 250 kPa

Liquid Flow rate(ml/min)	0 inHg	10 inHg	15 inHg	20 inHg
0.1	0.00127	0.00154	0.00168	0.00182
0.05	0.00124	0.00152	0.00166	0.00180
0.009	0.00123	0.00150	0.00164	0.00178
0	0.00122	0.00150	0.00164	0.00178

Table A.4: The simulated flux of CO_2 entered the outer tube(J_2) at different vacuum pressure. Gas pressure is 150 kPa

Liquid Flow rate(ml/min)	0 inHg	10 inHg	15 inHg	20 inHg
0.1	0.00033	0.00059	0.00072	0.00085
0.05	0.00035	0.00060	0.00073	0.00086
0.009	0.00036	0.00061	0.00074	0.00086
0	0.00036	0.00061	0.00074	0.00087

Table A.5: The simulated flux of CO_2 entered the outer tube(J_2) at different vacuum pressure. Gas pressure is 200 kPa

Liquid Flow rate(ml/min)	0 inHg	10 inHg	15 inHg	20 inHg
0.1	0.00070	0.00096	0.00109	0.00122
0.05	0.00072	0.00097	0.00110	0.00123
0.009	0.00073	0.00098	0.00111	0.00124
0	0.00074	0.00099	0.00111	0.00124

Table A.6: The simulated flux of CO_2 entered the outer tube(J_2) at different vacuum pressure. Gas pressure is 250 kPa

Liquid Flow rate(ml/min)	0 inHg	10 inHg	15 inHg	20 inHg
0.1	0.00107	0.00133	0.00145	0.00158
0.05	0.00109	0.00134	0.00147	0.00160
0.009	0.00110	0.00136	0.00148	0.00161
0	0.00111	0.00136	0.00149	0.00161

Experimental data. The inlet flux of CO_2 (J_1) is showed in the tables (Table A.7-A.9).

Table A.7: The experimental inlet flux of CO_2 (J_1) at different vacuum pressure. Gas pressure is 150 kPa

Liquid Flow rate(ml/min)	0 inHg	10 inHg	15 inHg	20 inHg
0.1	0.00044	0.00053	0.00057	0.00062
0.05	0.00044	0.00052	0.00057	0.00062
0.009	0.00043	0.00051	0.00057	0.00061
0	0.00042	0.00051	0.00056	0.00061

Table A.8: The experimental inlet flux of CO_2 (J_1) at different vacuum pressure. Gas pressure is 200 kPa

Liquid Flow rate(ml/min)	0 inHg	10 inHg	15 inHg	20 inHg
0.1	0.0006	0.00073	0.00079	0.00083
0.05	0.0006	0.00072	0.00078	0.00083
0.009	0.00059	0.00071	0.00077	0.00082
0	0.00058	0.00071	0.00077	0.00082

Table A.9: The experimental inlet flux of CO_2 (J_1) at different vacuum pressure. Gas pressure is 250 kPa

Liquid Flow rate(ml/min)	0 inHg	10 inHg	15 inHg	20 inHg
0.1	0.00085	0.00094	0.001	0.00105
0.05	0.00085	0.00094	0.00099	0.00104
0.009	0.00084	0.00093	0.00098	0.00103
0	0.00083	0.00092	0.00098	0.00103